

The kinematics of the bulge and the disc of NGC 7331

Roelof Bottema

Kapteyn Astronomical Institute, P.O. Box 800, NL-9700 AV Groningen, The Netherlands, e-mail:robot@astro.rug.nl

Received date1; accepted date2

Abstract. Results are presented of spectroscopic emission and absorption line observations along the major axis of the Sb galaxy NGC 7331. The kinematics of the ionized gas and stellar component are derived, being regular and symmetric with respect to the centre of the galaxy. Contrary to what may be expected, for $R \lesssim 40''$ the emission line gas appears to rotate slower than the stars. A likely explanation for this phenomenon is an inclined and warped gas layer in those inner regions. In the bulge dominated region the absorption line profiles are asymmetric in the sense that they have a shallow extension towards the systemic velocity. No counterrotating stellar component is observed which is contrary to previous claims. As demonstrated, these claims might be based on a wrong interpretation of the employed analysis method. Outside the bulge dominated region the stellar radial velocities are in agreement with the neutral hydrogen dynamics and the stellar velocity dispersion decreases towards larger radii.

A detailed bulge/disc light decomposition has been made. That has been used to construct a kinematical model of NGC 7331 from which model absorption line profiles were calculated. These profiles have been compared with the observations and model parameters have been adjusted to obtain a good match. It appeared necessary to combine a rapidly rotating disc having a radially decreasing velocity dispersion with a slowly rotating constant dispersion bulge. Then, simultaneously, the observed stellar radial velocities, the velocity dispersions and the observed asymmetry of the line profile could be explained satisfactorily. An even better fit to the data can be achieved when the disc is relatively thinner and colder inside the bulge region.

For the disc the stellar velocity dispersions and photometry result in a mass-to-light ratio of $1.6 \pm 0.7 M_{\odot}/L_{\odot}^I$. This value agrees with previous determinations for other discs using observed velocity dispersions. A rotation curve analysis allows the calculation of the mass-to-light ratio of the bulge which amounts to 6.8 in the I-band; considerably larger than the disc value. It appears that the mass distribution of NGC 7331 is completely dominated by the combination of bulge and dark halo at all radii. Comparing well determined mass-to-light ratios of a number of bulges

with disc values, on average, $(M/L)_{\text{bulge}}$ is three times as large as $(M/L)_{\text{disc}}$ in the I-band. For the B-band this ratio goes up to 7.2, a fact which should have cosmological consequences.

Key words: galaxies: individual: NGC 7331 – ISM: kinematics and dynamics – galaxies: fundamental parameters – galaxies: kinematics and dynamics – galaxies: spiral

1. Introduction

Beyond the optical edge of disc galaxies large amounts of dark matter are needed to explain the flat rotation curves determined from the velocity field of the H I gas (Bosma 1978; Begeman 1987). However, the contribution of the luminous disc matter to the total rotation cannot be determined from a rotation curve analysis (van Albada et al. 1985). On the other hand, knowing the surface density of the disc allows the construction of the rotation curve of the disc only. Comparison with the observed total rotation then gives the rotational contribution of the disc. Galactic discs can essentially be described as locally isothermal stellar sheets embedded in a dark halo. Measuring the stellar velocity dispersion of the disc then provides the surface density to determine this rotational contribution.

For a dozen galactic discs these velocity dispersion measurements have been done (Bottema 1993, and references therein) though for most of these only over a limited radial extent. The general conclusion is that a galactic disc provides, at the position of the maximum rotation of the disc, $63\% \pm 10\%$ of the total rotation of a galaxy (Bottema 1993, hereafter B93). Using an analysis of the light and colour distributions of galactic discs this conclusion can be rewritten to $(M/L)_B = 1.8 \pm 0.4$ when $B - V = 0.7$. For a disc with a certain brightness and colour a general expression is determined for its rotational contribution and for its mass-to-light ratio (Bottema 1997). Unfortunately the error on the mass-to-light ratio is still large caused by the small sample of discs for which dispersions have actually been measured. Consequently an extension of the sample is badly needed.

There are other problems which can be addressed when disc dispersions are better known, for instance galaxy formation. Nowadays it is believed that a collapse of dark matter creates the potential well in which baryons collect to form a galaxy (e.g. Katz & Gunn 1991). To check if this scenario is right and to understand the details, it is necessary to know the dark to luminous mass ratio in present day galaxies (Dalcanton et al. 1997; Mo et al. 1997). In addition a theoretical basis can then be provided for the Tully-Fisher relation (Tully & Fisher 1977; Rhee 1996a, 1996b).

Already in 1973 Ostriker & Peebles showed that a cold isolated disc is highly unstable to bar formation. More stable discs can be made by putting them in a large amount of spherical (dark) matter or when discs are hot. The observations of the stellar velocity dispersions show that the latter is not valid. Consequently dark matter is needed to stabilize discs, but how much? Numerical calculations are well suited to investigate this problem. Simulations by Efsthathiou et al. (1982), Bottema & Gerritsen (1997), and Syer et al. (1997) show that the mass contribution of a stable disc must be well below the so called maximum disc hypothesis (van Albada & Sancisi 1986) situation. This is in perfect agreement with the results of the stellar dispersion measurements. On the other hand, stabilization of discs may be taken over by a massive central bulge. Can a bulge maybe be considered as a luminous extension of a dark halo?

Galactic bulges have a global isothermal nature in the sense that the observed velocity dispersion is rather uniform over the bulge's extent. Bulges can be described consistently with models of isotropic oblate spheroids (Kormendy & Illingworth 1982; Jarvis & Freeman 1985), or in other words as rotationally flattened isothermal spheres.

Galaxies with morphological type ranging from Sa to Sb are equipped with both, a disc and a bulge, and consequently there is a region where these will overlap. One may expect that the different kinematical properties of bulge and disc, as observed where one or the other is dominant, are maintained when both are present. This was suggested by absorption line observations of the Sb galaxy NGC 2613 (Bottema 1989). This galaxy has a bulge which appears to be somewhat displaced from the centre and on one side clear double peaked line profiles are observed reminiscent of bulge and disc having a different rotation. Such a scenario has also been suggested by Kuijken & Merrifield (1993, hereafter KM93) to explain the asymmetric absorption line profiles of the galaxy UGC 12591. An asymmetric profile can be made as a superposition of a low dispersion rapidly rotating disc and a higher dispersion more slowly rotating bulge; KM93 show in a quantitative way that this can explain the UGC 12591 observations. To investigate the stellar kinematics in the bulge-disc transition region I obtained absorption line spectra of the Sb spiral NGC 7331. The data were lying on the shelf for a while when the discovery of a counterrotating bulge of NGC

7331 was announced (Prada et al. 1996, hereafter P96). This renewed my interest in this galaxy and motivated the examination of the data.

Since the first detection of a counterrotating component in an elliptical galaxy (Franx & Illingworth 1988) a frantic search for more counterrotating galaxies started in the astronomical community. It appeared that counterrotation in elliptical galaxies is not uncommon which, in fact, is not unexpected considering the likely merger history of ellipticals. In later type galaxies, however, counterrotation is rare; known to date are NGC 4550, of type E7/S0 (Rix et al. 1992), NGC 4826 of type Sab (Braun et al. 1992; Rix et al. 1995) and NGC 4138 of type Sa (Jore et al. 1996). Also claimed to possess a counterrotating component is the Sb galaxy NGC 7217 (Kuijken 1993; Merrifield & Kuijken 1994) although inspection of the line profiles shows that a kinematic asymmetry by a bulge/disc situation is more likely (see also the discussion in the remainder of this paper). P96 find a counterrotating component in the Sb galaxy NGC 7331, at the 15% intensity level, counterrotating with 50 km s^{-1} and this component is dynamically cold. That poses a problem; how can two cold components exist together, one rotating with $\sim 250 \text{ km s}^{-1}$ (the disc) and the other with 50 km s^{-1} , in the same potential? A more detailed analysis is certainly warranted. In addition to the kinematics in the transition region also the velocity dispersions of the disc and the bulge can be determined. From this the mass-to-light ratios of the components can be calculated and be compared with each other.

NGC 7331 is a massive Sb spiral galaxy. Photometry exists in the r-band (Kent 1987) and HI observations have been obtained and analysed by Begeman (1987) and Begeman et al. (1991). The neutral hydrogen shows a regular velocity field and rotation speeds up to 257 km s^{-1} . A photograph of the galaxy is given in Fig. 1, where NGC 7331 appears to be a regular and undisturbed system. The adopted distance of 14.9 Mpc is in perfect agreement with the value of $15.1 \pm 1.0 \text{ Mpc}$ determined recently from Cepheid variables (Hughes et al. 1998). For convenience a summary of the main parameters is presented in Table 1.

2. Observations and data reduction

2.1. The observations

The spectroscopic observations were carried out on September 19 and 20, 1987, at the observatorio de Roque de los Muchachos on the island of La Palma, using the Isaac Newton (2.5 m) telescope. The intermediate dispersion spectrograph was used at the Cassegrain focus. This spectrograph had a grating of 1200 groves per mm, a camera with a focal length of 235 mm (Wynne 1977) and slit width of $220 \mu\text{m}$ ($= 1''.19$ on the sky). In that way a spectrum is produced with a full width at half maximum (FWHM) velocity resolution of $\sim 70 \text{ km s}^{-1}$, centred at

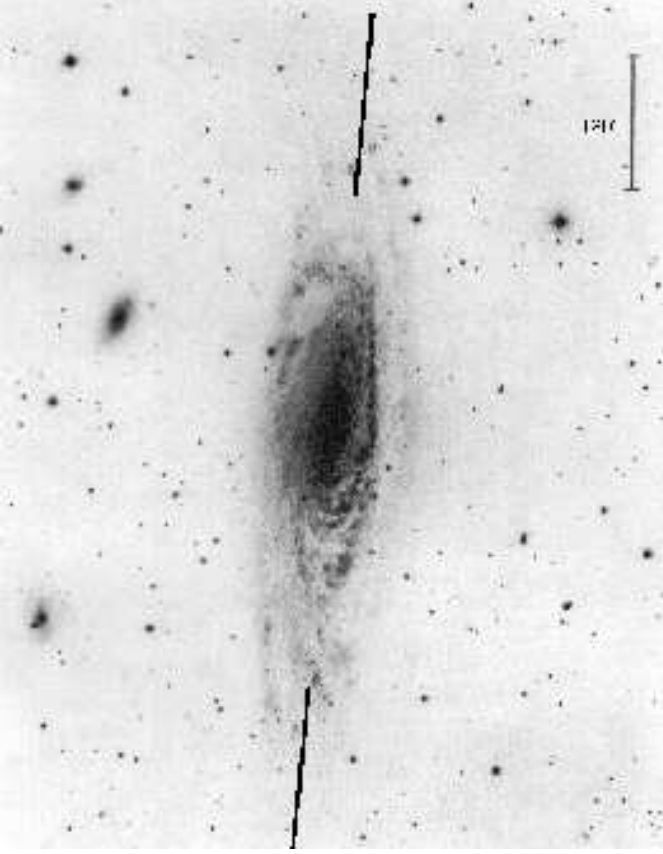


Fig. 1. Reproduction of the optical image of NGC 7331 from the Shapley-Ames catalog (Sandage & Tammann 1981). Spectroscopy is obtained along the whole major axis at the position of the left out part of the indicated line. North at top, East at left.

Table 1. Description of NGC 7331

R.A. (1950)	22 ^h 34 ^m 47 ^s	<i>a</i>
Declination (1950)	34° 09′ 30″	<i>a</i>
Hubble type	Sb(rs)I-II	<i>a</i>
Inclination	75°	<i>b</i>
Pos. angle major axis	172°	<i>b</i>
Total H I mass	11.3 10 ⁹ M _⊙	<i>b</i>
Systemic velocity	820 ± 3 km s ⁻¹	<i>b</i>
Abs blue magn. $B_T^{o,i}$	-21.73	<i>c</i>
Distance	14.9 Mpc	adopted
Unit conversion	1″ = 72.24 pc	

a Sandage & Tammann (1981)

b Begeman (1987)

c from Sandage & Tammann, for adopted dist.

a wavelength of 5162 Å. The data were recorded with the Image Photon Counting System (IPCS), having a wavelength range from 4634 to 5691 Å, divided up into 2040 pixels. The spatial extent on the sky was covered by 82 consecutive spectral rows each of size 2″.92, resulting in a

total extent of nearly four arcminutes. During the observations the seeing was considerably smaller than the size of a spectral row, leaving them all uncorrelated. On both nights the slit was put parallel to the major axis, at a position angle of 352° with the nucleus falling in the slit. One night the northern part of the galaxy was covered with the nucleus at row 13, lying 38 arcseconds from the edge of the slit. Although in this case also a part of the south side is covered, in the remainder of this paper the results from this observation will all be referred to as “North side”. On the second night the southern part was covered with the nucleus being positioned 2″.3 beyond the end of the slit. Results from this observation will be referred to as “South side”.

The total exposure on the North side lasted for 21 000 seconds (= 5^h 50^m) and on the South side for 24 000 seconds (= 6^h 40^m). These exposures were divided up into single exposures of 1500 seconds, preceded and succeeded by the observation of a Cu-Ne calibration lamp. In addition spectra of 7 template stars all of type close to K0III were recorded, of course using exactly the same instrumental configuration and wavelength calibration. Furthermore observations of the twilight sky and dark current were made.

2.2. Data handling

For all the individual 2-d spectral images of the galaxy, the encompassing Cu-Ne lamp exposures were added. The wavelength calibration was performed by using 22 emission lines spaced over the 1057 Å interval. The standard deviation of the lines from the final wavelength solution was never larger than four to five km per second. Next the data were regridded to a common log λ scale (30.2 km s⁻¹ per pixel) and added to form two, North side and South side, calibrated spectral images. For the template star exposures the same procedure was followed. The calibrated stellar spectra were shifted to one common redshift and after this, all spectra were averaged to produce one essentially noise free template spectrum.

The flatfield exposures registered on the twilight sky showed that the pixel-to-pixel variation was less than 2%, being so small that no corrections were necessary. The twilight exposures were averaged together and along the wavelength direction, providing the response along the slit. The dark current subtracted images were corrected for this response. There was no detectable S-shape distortion and consequently no corrections to remove such a distortion were necessary. To get an impression of the count levels of the two galaxy spectra, in Fig. 2 the average number of counts over the wavelength range is shown along the slit.

The Hβ and [O III] 5007 Å and 4959 Å lines were clearly visible in the spectra. The forbidden oxygen lines continued all the way to the centre of the galaxy, while Hβ emission was essentially lost in the Hβ absorption for radii

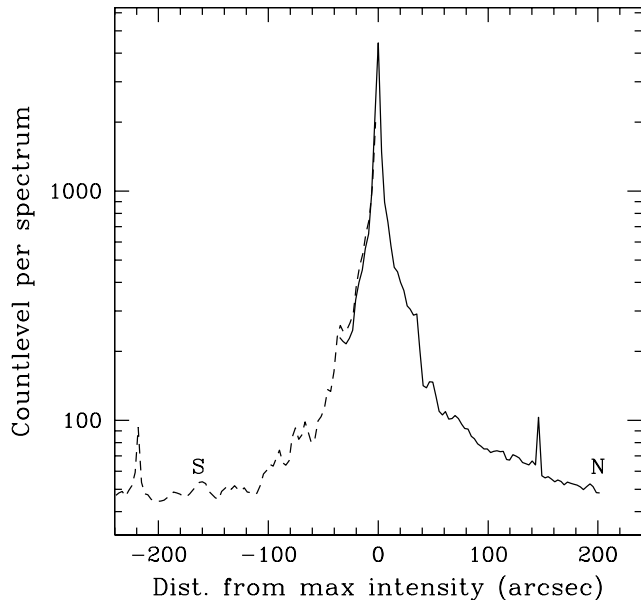


Fig. 2. The count level along the spectrograph slit. Given is the average over 2040 wavelength pixels per $2''.92$ on the sky. The light of the sky is not subtracted.

less than ~ 20 arcseconds. The emission line kinematics was determined by fitting gaussians to the profiles. When necessary spectra were averaged along the slit to increase the S/N. Also for the absorption lines spectra had to be averaged along the slit to obtain a sufficient S/N. Each spectrum has a certain position along the slit corresponding to a fixed position on the galaxy or sky. At every position of every spectrum, encompassing spectra were added until a count level of galaxy emission of at least 200 was reached. In this way, for larger distances from the centre spectra become correlated but remain evenly distributed with separation of $2''.92$. Furthermore the S/N decreases at larger radii because of the constant level of sky and dark current emission. When averaged in this way, the resulting spectrum is weighted according to the intensity level of the individual spectra; the position along the slit is (except in Fig. 4) then also given as the intensity weighted position.

Next the continuum level was determined by fitting a fifth order polynomial to the whole spectrum and was subsequently subtracted. In this way one loses the line strength information but the spectrum will not suffer from division by a number close to zero. At positions of the emission lines and strong skylines, spectra were put at a zero level such that those positions will not contribute to the cross-correlation sum. Certainly on the North side and to a lesser extent on the South side there is not a sufficient slit section free of galaxy light. Hence it is not possible to obtain a clean sky spectrum and consequently the sky was not subtracted. For the present case this does not pose a large problem. At first because all the radial velocities of

NGC 7331 are substantially redwards from the solar radial velocity, and no blending of the line profiles of galaxy and the sun (=sky) can take place. Secondly the amount of light from the galaxy is still large enough compared to that of the sky, that a continuum level sufficiently appropriate for the galaxy light can be determined. As for the galaxy, from the template spectrum the continuum level was subtracted.

The cross correlation functions have been calculated between the spectral rows of the galaxy and the template spectrum. This is done by using Fourier techniques. In general the continuum subtraction by means of the polynomial fit is not sufficient and additional low frequency wavenumbers have to be, and in the present case were, filtered out. Insufficient filtering shows up immediately as a continuum level offset between the cross correlation function and the auto correlation function of the template. Care has been taken that such an offset did not appear. Except for the $H\beta$ absorption line and small regions where [O III] and skylines were present, the whole spectral range was included in the cross correlation sum. This range contains a forest of hundreds of absorption lines of which the most striking are the Mg triplet around 5170 \AA and the Fe/Ca complex around 5250 \AA .

2.3. Determining the stellar kinematics: the cross-correlation-clean technique

Until this point the data handling is rather standard, but for getting out the actual stellar kinematics a number of different methods have been and are being used. All assume that the observed galaxy spectrum can be represented by that of a suitable template spectrum convolved with the galaxy broadening function, also called galaxy line profile. Thus to obtain this line profile always some kind of deconvolution is involved. The first methods to be used are those by Illingworth & Freeman (1974) and by Sargent et al. (1977), applying a division in Fourier space, and the one by Tonry & Davis (1979), applying a cross-correlation technique. Later on other and improved methods have been used (a.o. Bender 1990; Rix & White 1992; Franx & Illingworth 1988; van der Marel & Franx 1993; KM93; Statler 1995) establishing a situation where every author(s) uses his own method. In general all such methods are being applied to elliptical galaxies or bulges, where one has a nearly constant velocity dispersion and a large surface brightness. For galactic discs, however, the surface brightness is lower and the velocity dispersion decreases towards larger radii. In such situations Bottema (1988) has used a method which remains as closely as possible to the original data. One can show that the cross-correlation function (hereafter: ccf) of template and galaxy spectra is equal to the convolution of the galactic line profile with the auto-correlation function (hereafter: acf) of the template spectrum (Bottema et al. 1987). Displaying the ccf then gives one directly the line profile, albeit convolved with a

symmetric acf. By fitting a grid of acfs broadened to different dispersions Bottema (1988) extracted the relevant radial velocities and velocity dispersions. This method is straightforward and the fitting can be inspected graphically, but the error analysis had to be done by eye and asymmetric line profiles could not be accommodated for.

Therefore this method has been improved. In order to extract the line profile, the ccf is deconvolved using the CLEAN technique (Högbom 1974), with the template acf as beam or point spread function (see also Franx & Illingworth 1988). Certainly for barely resolved signals with substantial amounts of noise added such a cleaning technique proves to be a superior deconvolution method. Hence it can be applied with confidence for the narrow, noisy, line profiles typical for galactic discs. Clean components have been subtracted for a region around the peak of the ccf until a residual well below the noise level. The line profile was then restored by convolving the components to a gaussian function with a dispersion of $2\frac{1}{2}$ velocity pixels and by adding the residuals. The width of this gaussian was determined as a compromise between more resolution and more noise for a narrower gaussian and less resolution with less noise for a broader function. In theory, if there is no noise, one could make the restoring function as narrow as allowed by the sampling criterion; down to a dispersion of approximately one pixel.

When a deconvolved line profile is obtained it can in principle be parameterized in any way. Presently it was chosen to fit in first instance a gaussian to the profile, even if it is not symmetric. The radial velocity is given by the position and the stellar velocity dispersion by the gaussian dispersion from which the (restored) resolution has been subtracted quadratically. Errors of the parameters are obtained from the usual least squares fitting procedure. By fitting such a single gaussian to the profile the position and dispersion are extracted in a way similar to that of the conventional methods, allowing an easy comparison and understanding. In the case of NGC 7331 skewed profiles are observed and consequently more parameters are needed to describe the profile. Well suited appeared to be the Hermite polynomial analysis by van der Marel & Franx (1993). Only one additional asymmetric (*h3*) parameter was considered, resulting in a least squares fitting of the function

$$f(v) = ae^{\frac{-(v-b)^2}{2c^2}} \left\{ 1 + h3 \left[1.1547 \left(\frac{v-b}{c} \right)^3 - 1.1732 \left(\frac{v-b}{c} \right) \right] \right\}, \quad (1)$$

to the line profile. Here v is the radial velocity and a, b, c , and $h3$ the parameters to be determined. There are two matters to be noted. At first, the values of a, b , and c are not completely, but nearly equal to the parameters obtained from a straight fit of a gaussian to the profile (see

van der Marel & Franx for a discussion). In practice, to the line profile both, a gaussian and the function given by Eq. (1) is fitted. But when results are presented a, b , and c are not given, only the gaussian fit parameters. Secondly, *h3* does not give the skewness of the actual line profile, but the skewness of the resolution broadened profile. When analysing the observations this should be taken into account.

3. Observational results

3.1. The emission lines

The radial velocities determined from the $H\beta$ and [O III] 5007 Å line are presented in Fig. 3, together with the radial velocities inferred from the HI rotation curve (Begeman 1987; Begeman et al. 1991). As can be seen, the velocities of the three emission lines are in excellent agreement. In the central region, for $R \lesssim 40''$ there is no HI gas and consequently no HI rotation curve. $H\beta$ is observed somewhat further inwards until approximately $30''$. On the other hand the oxygen line (although weak) continues all the way to the centre. In general bulges do not show any significant emission lines. For NGC 7331 this indicates that the disc, or some other young galactic component is present in the centre, embedded in the bulge. To check whether the oxygen emission indeed originates from a cold component and not, for instance, from bulge planetary nebulae, the [O III] velocity dispersion was measured. Only at the very centre, for radii less than five arcseconds this line is broadened to $100 \pm 20 \text{ km s}^{-1}$. Outside this radius the line is unresolved meaning a dispersion of less than $\sim 30 \text{ km s}^{-1}$.

A comparison was made with the radial velocities along the major axis of the $H\alpha$ and [N II] line as measured by Afanasiev et al. (1989). Their data are confined to within 60 arcseconds from the centre, but have a much better spatial sampling than for the present observation. Except for the usual absolute calibration error the velocities are in exact agreement, for instance the velocity feature at $-18''$ is present in both observations. A comparison with the observations of Rubin et al. (1965) also shows agreement, although a detailed comparison is not possible because slit positions do not coincide completely.

3.2. The stellar, absorption line kinematics

To illustrate the appearance and quality of the absorption line kinematics all the cleaned line profiles along the major axis are presented in Fig. 4. This image is constructed using the averaging procedure along the slit as discussed in the previous section. Therefore the indicated distances from maximum intensity of the individual line profiles are the distances of the spectra around which regions have been averaged, in an intensity weighted way. So these distances may differ slightly from the actual distance to the

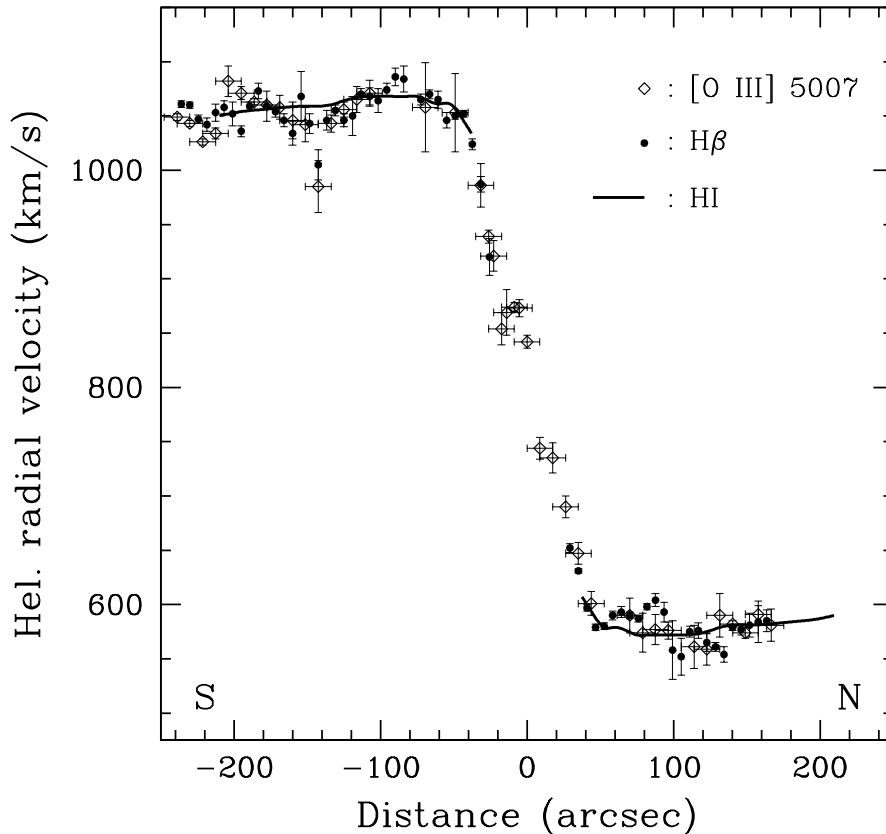


Fig. 3. Observed radial velocities of the $H\beta$ and $[O\ III] 5007\ \text{\AA}$ emission lines compared with the radial velocities inferred from the HI rotation curve. In the inner $40''$ there is no neutral hydrogen gas and only very little $H\beta$ emission.

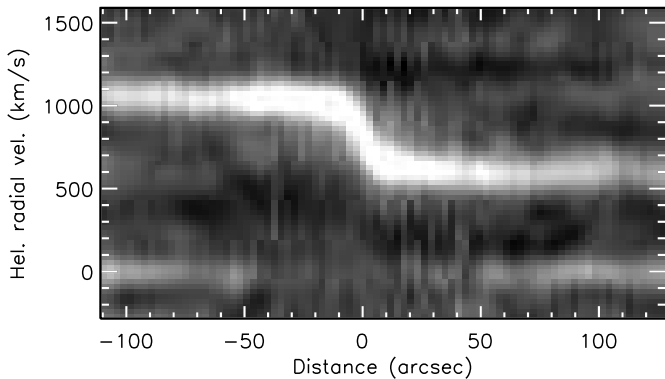


Fig. 4. The stellar absorption line profiles along the major axis. For distances within $40''$ from the centre, the line profiles are skewed; there is a shallow extension towards the systemic velocity. Note the signature of the sky at zero radial velocity.

centre. North and South side have been combined on integer spectra while in reality there is a 0.2 spectral size (of $2''92$) shift. But these small approximations will not generate any significant deviation from the actual appearance of the position velocity diagram.

The autocorrelation function of the template exhibits some corrugation along the velocity direction. Most of this corrugation has been cleaned away but some residual re-

mains as can be seen in Fig. 4. In fact, this is to be expected because the template spectrum can never be a perfect match to the spectrum of the stellar population of the galaxy. Any absorption line interpretation procedure suffers from this shortcoming, but this can only be seen by displaying matters as in Fig. 4. Looking at the figure one can thus notice a small gully at the high and low end of the galaxy's radial velocities. Also some vague reflection patterns are apparent. The magnitude of these irregularities is small, however, always below the noise level determined from line free regions surrounding the galactic emission. In addition one may note the signal of the solar spectrum at a radial velocity of zero.

By fitting a gaussian to the line profiles the stellar radial velocities and dispersions are determined. The first are presented in Fig. 5, together with the HI radial velocities and emission line velocities, the latter given by a hand drawn line through the data points of Fig. 3. The velocity dispersions are presented in Fig. 6, top panel. At the centre dispersion values around $130\ \text{km s}^{-1}$ are reached, while for larger radii the dispersion decreases, similar for both sides of the galaxy. In the lower panel of Fig. 6 the $h3$ parameter is displayed following from a fit of Eq. (1) to the profiles. Like the dispersion this asymmetry parameter is symmetric and regular with respect to the centre of the galaxy.

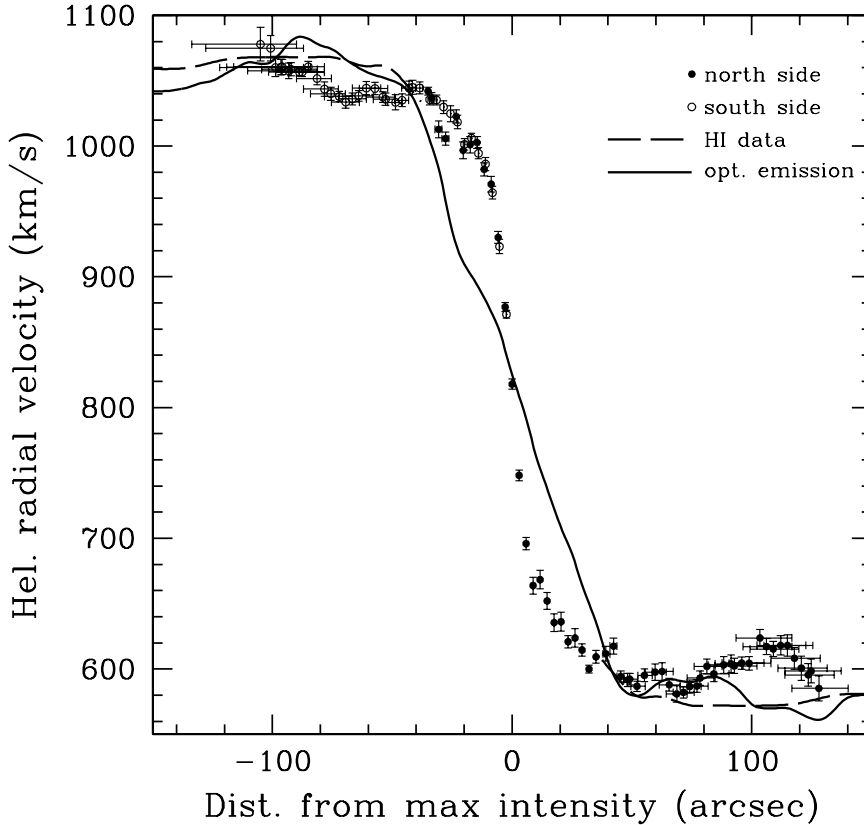


Fig. 5. Stellar radial velocities compared with the emission line velocities. The full drawn line is a fit by eye to the $H\beta$ and $[O\ III]$ data of Fig. 3. Contrary to what is expected, in the inner regions, the gas appears to rotate slower than the stars.

3.3. Discussion of the observed kinematics

From Fig. 5 it will be immediately obvious that for radii $\lesssim 40''$ the emission line gas appears to rotate slower than the stars. This is puzzling. One would expect the contrary; caused by asymmetric drift and integration effects a regular galaxy shows, in general, a stellar rotation lower than that of the gas. That is to say, the stars rotate slower than the “potential” rotation or testparticle rotation (= rotation of a testparticle in the plane: $v_t = \sqrt{-R \partial\Phi/\partial R}$). For a galaxy the emission line gas should rotate as testparticles and consequently for NGC 7331 the velocity aberration of this emission line gas is even larger than the observed velocity difference between stars and gas. For example at a radius of ten arcseconds the gas rotates more than 107 km s^{-1} too slow, which amounts to nearly a factor of two. How can this be explained?

One might imagine a barred situation. It is known that stars (Miller & Smith 1979; Hohl & Zang 1979) and gas (Athanasoula 1992, and references therein) have substantial non circular streaming motions along the bar. But at first it is hard to imagine how the gas motion might differ so substantially from the stellar motion. For instance the analysis by Athanasoula (1992) shows that the gas motion in a bar largely follows the x_1 and x_2 stellar orbits. Secondly the I and K band photometry of the central

regions by P96 does not indicate any significant barred morphology. Hence the explanation by a bar is unlikely.

Another possibility is that the gas ends, going inwards, in an edge-on gas ring at $R \sim 50''$. Such a situation will give the kinematical appearance of a solid body rotator as observed inside this radius. However, given the need for a sudden inclination change from 75 to 90 degrees combined with the need for the gas to end at the same position, this explanation seems remote.

A slower apparent (gas) rotation can, of course, be produced by a more face-on orientation of the plane in which the gas is rotating. To produce the difference between gas and stellar velocities as observed, it is then necessary that from approximately $40''$ inwards the gas plane is increasingly more inclined with respect to the plane of the galaxy. Such an inner warped structure could have been generated by a gascloud or gas rich dwarf galaxy which has fallen in on an orbit with some angle with respect to the plane of the galaxy. Numerical calculations show that certainly the gas will then quickly settle into the centre of the galaxy. This explanation is a theory which works in principle. However, to prove or disprove it will not be straightforward; observations of the emission line gas other than along the major axis are needed. A different observation which supports the hypothesis of a warped gas layer is that of the inclined gas ring or disc inside the bulge of

M31 (Boulesteix et al. 1987), a galaxy similar in appearance as NGC 7331.

Another point to be noted is the irregular behaviour along the slit of both the stellar radial velocities and dispersions. For example the stellar rotation is different on both sides near a radius of $100''$. Also at those positions the difference between gas and stellar rotation is different for both sides and in addition the velocity dispersion suddenly increases over there. This can only mean that in some regions of this galaxy stars and gas have not yet formed a relaxed configuration. Is this kinematical appearance of NGC 7331 unusual? No, it is not. The stellar kinematics of large galaxies is in general more irregular than that of smaller galaxies. These matters are discussed by Bottema (1993) arguing that the irregularity could be the result of more or less recent capture of small matter clumps by large galaxies.

3.4. No counterrotation

Both, the image of the line profiles in Fig. 4, and the $h3$ parameter in Fig. 6 show that for radii less than $40''$ the line profiles are asymmetric; they have a regular and shallow extension towards the systemic velocity. Using a modified version of the Unresolved Gaussian Decomposition method (KM93) P96 find for the same object a double line profile interpreted by them as a counterrotating bulge. This double profile is found between radii of 5 to 20 arcseconds on both sides along the major axis. There is one dominant component at the normal galactic radial velocities. Another component at a 15% intensity level of the dominant peak is counterrotating with approximately 60 km s^{-1} and is unresolved by their spectrographic setup, meaning a velocity dispersion less than $\sim 50 \text{ km s}^{-1}$. Compared to the bulge dispersion of 125 km s^{-1} this component is cold. A close inspection of P96's profiles shows that although the counterrotating component is barely above the 1σ noise level, it is present in a number of independent spectral rows.

In this study such a counterrotating component is not observed. Then we have the uncomfortable situation that different analyses of the same object give different results. How is that possible? To check if some kind of error has been made using the present method of interpreting the data a close inspection was made of the original cdfs. The same asymmetry at radii $< 40''$ is obvious but there is no extra component. Hence the clean procedure did not make appear or disappear any features. Because the cross-correlation procedure gives you directly the line profiles it is not likely that such a counterrotating component really exists. Note that P96 have nearly the same instrumental resolution, but spectra are taken around 8500 \AA instead of the present 5100 \AA . Could P96 have done something wrong? To investigate this the UGD algorithm has been applied to the present North side spectra. The same UGD setup with a two pixel dispersion and three pixel separa-

tion of the gaussians is used as by P96, and with nearly equal velocity pixel sizes both analyses should be comparable. And the result? Also a counterrotating separate line profile is found at the 20% level of the main profile between radii of 10 and $40''$ counterrotating with 50 km s^{-1} .

The analysis of P96 differs slightly from the standard UGD algorithm. They use a two dimensional version of UGD where just as in the dispersion direction, also in the spatial direction gaussian components are fitted with a dispersion of 2 pixels and separation of 3 pixels. This imposes extra smoothness and noise suppression (Binney & Merrifield 1998). But, frankly, I do not see that such a procedure is much different from a simple smoothing along the spatial direction, giving better S/N and poorer resolution. P96 point out that: "in general, the results of both algorithms (UGD and 2dUGD) are the same". As demonstrated above, the original UGD algorithm indeed gives the same result as found by P96 and consequently in the present discussion it should not matter whether the 1dUGD or 2dUGD procedure is used.

Anyway, the UGD method generates a counterrotating component while the cross-correlation clean (CCC) method only produces an asymmetric profile. A more detailed comparison between the two methods has been performed, doing some test analyses on skewed profiles. A description of this investigation is given in the Appendix. It appears that the counterrotating component is most likely an aliasing feature produced by UGD. When errors are superposed on the lineprofile as calculated by UGD, this feature is not significant and should have been discarded. So, UGD is not wrong, but by omitting the presentation of the errors P96 may have been led to a wrong interpretation of the results.

4. The bulge/disc light decomposition

4.1. The observed photometry

To interpret the observations a dynamical model of NGC 7331 will be constructed. For this a description is necessary of the luminosity distribution of the bulge and the disc which have to be derived from the photometry. In the present case such a procedure is not straightforward.

Photometry in the Thuan & Gunn (1976) r-band is obtained by Kent (1987). Unfortunately a bulge/disc light decomposition according to Kent's procedure is not possible because the apparent ellipticity of the bulge and disc are equal. Therefore one has to resort to the classical method of assuming a certain density behaviour of one of the components, fit this behaviour there where this component is dominant and subtract to get the density of the other component. For example Kent (1987) assumes an exponential bulge with scalelength of approximately 0.8 kpc, which he subtracts from the total photometry to get the disc light. In the rotation curve analysis by Begeeman et al. (1991), for the same photometry a disc with

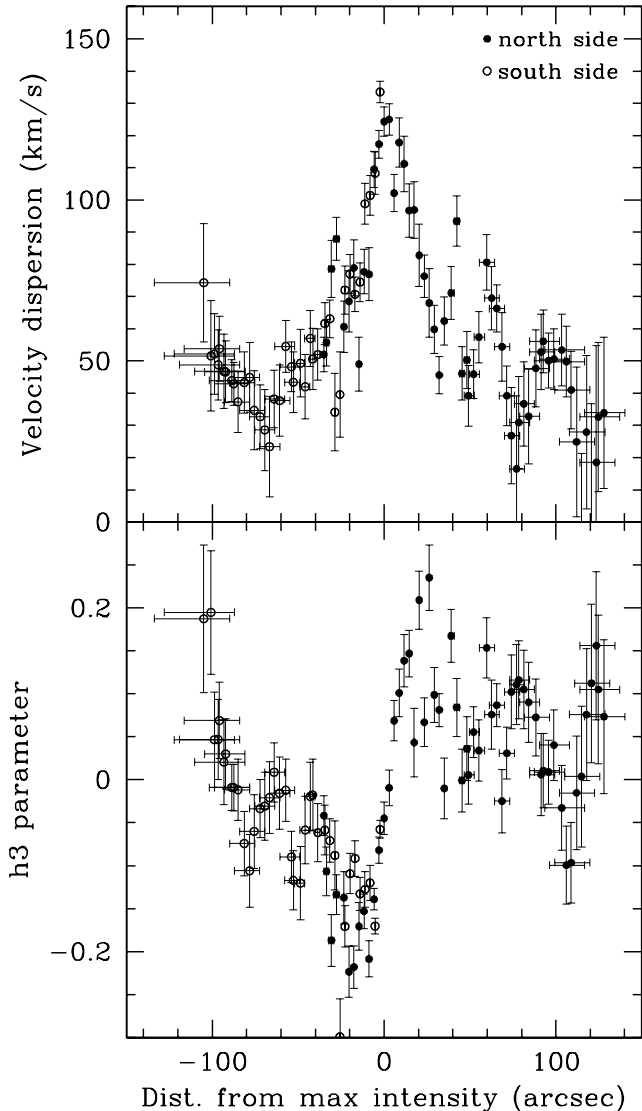


Fig. 6. Stellar velocity dispersions and absorption line asymmetry ($h3$) parameter along the major axis. Both show a regular and symmetric behaviour with respect to the centre.

scalelength of $62''$ has been fitted to the outer regions. Subtraction of the disc gives the bulge light and a bulge to disc light ratio of ~ 1.4 , which is too large for this galaxy.

Photometry of the inner regions in the I and K bands is presented by P96. Although P96 argue for a different radial behaviour in K and I, in reality, overlaying the two profiles shows that both are nearly identical over the radial extent where both have been measured. In the remainder of this paper the I band photometry of P96 will be used.

The r-band observations show a constant ellipticity ε of 0.6 for the whole galaxy. In the I and K band, however, the central regions show a tendency towards a rounder

situation. Fig. 2 of P96 gives the ellipticity along the major axis. For radii larger than $15''$ $\varepsilon = 0.6$ consistent with Kent’s photometry; going inwards, the ellipticity decreases gradually to $\varepsilon = 0.4$ at $5''$ and to $\varepsilon \sim 0.1$ near the centre. Apparently there is a nearly spherical distribution very close to the centre.

4.2. The “large” and “small” bulge

There remains the decomposition problem. Initially two extreme bulge/disc ratios were chosen expected to encompass the range of possibilities. These ratios or situations will be referred to as “large” bulge and “small” bulge. The large bulge was constructed in the following way: Stellar kinematical information is available till $R \sim 150''$; therefore a fit of an exponential disc was made to the outer range of this $150''$ resulting in a disc scalelength (h_d) of $43''$ and disc central (not corrected to face-on) surface brightness μ_0^I of $18.7 \text{ mag. arcsec}^{-2}$. This disc was subtracted from the total I-band photometry and to the remainder an $R^{1/4}$ law:

$$\Sigma^m(R) = 8.33 (R/R_e)^{1/4} + \Sigma_0^m, \quad (2)$$

was fitted, where Σ^m is the surface brightness in magnitudes, $\Sigma_0^m = \Sigma^m(R = 0)$, and R_e the effective radius. In this and forthcoming cases Eq. (2) always proved to be a good representation of the bulge light. Bulge and disc parameters are given in Table 2.

The smallest possible bulge contribution was determined as follows. If the bulge is spherical as indicated by the central ellipticity and the disc generates the larger ellipticity for $R > 15''$ then the bulge/disc transition should be near the middle of this radial extent. It appeared that such a situation can be achieved using an exponential disc with scalelength of $25''.5$ until $R = 60''$ and following the total light for $R > 60''$. A disc with this scalelength is equal to the disc fit of P96 to the K-band data, but that is a coincidence. Again the bulge was found by subtracting the disc from the total light and fitting an $R^{1/4}$ law, of which the parameters are also given in Table 2. This whole procedure constructing the large and small bulge may seem somewhat arbitrary and in fact it is. Still I feel confident that a good determination is given of the range of bulge/disc ratios; which may be judged by inspecting the graphical representation of the result given in Fig. 7.

4.3. The “lpd” bulge

Nevertheless when comparing the results of the models with the actual data, both large and small bulge did not give satisfactory results. Guided by experience obtained when doing this modelling it became clear that in fact a kinematical light decomposition could be made. That is to say, the narrow high velocity component of the line profile has to originate from the disc, while the broad underlying

Table 2. Bulge/disc decomposition parameters

bulge name	h_d (arcsec)	μ_0 (I-mag arcsec $^{-2}$)	R_e (arcsec)	Σ_0^m (I-mag arcsec $^{-2}$)	$c/l_d(0,0)$ (Eq. 3)
large	43	18.7	37	12.0	488
small	26.5 for $R < 60''$	17.7	15	10.9	432
lpd	see Fig. 7	see Fig. 7	39	12.7	31

component comes from the bulge. Therefore an estimate of the bulge/disc light ratio was made by considering the shape of the line profiles, all as a function of radius. Such a determination is not very precise, but the initial resulting b/d ratio already produced a better agreement between model results and data. Results were improved by increasing the initially estimated global b/d ratio with a factor two. In practice, the derived b/d ratio as a function of radius was applied to the I-band photometry producing a disc and bulge luminosity radial profile. Note that in this way both, the bulge and the disc radial light profile can be determined without any a priori constraint on the radial functionality. To the bulge profile again an $R^{1/4}$ law was fitted and then results a “line profile determined” bulge, or from now on “lpd” bulge, which is given graphically in Fig. 7. This lpd bulge has an effective radius comparable to that of the large bulge, while its surface brightness is lower (Table 2), which ensures that it falls between the two extremes considered above.

4.4. Deprojection

To put the bulge into a 3d model for the galaxy the $R^{1/4}$ bulge(s) have to be deprojected. For this a slight variation of the formula given by Young (1976) is used

$$l_b(r) = c \exp(-7.67 s^{1/4}) s^{-7/8} (1 + 0.11 s^{-1/4})^{-1}, \quad (3)$$

with

$$s = \frac{r}{R_e}, \quad (4)$$

where l_b is the luminosity density as a function of 3d coordinate r and R_e is the observed effective radius. In this case the bulge is assumed to be spherical. To check the influence of this assumption also situations with a flattened bulge (with $a/b = \text{major/minor apparent axis} = 2/1$) have been investigated. It appeared that the results of the stellar kinematical modelling are not sensitive to such changes of the bulge morphology. Bulge and disc were put in a 3d situation and integrated along the line of sight to determine the constant of proportionality $c/l_d(0,0)$ (c from Eq. (3) and $l_d(0,0)$ the central luminosity density of the disc) by comparison with the observed b/d light ratios along the major axis for the different situations. The resulting value is given in Table 2.

4.5. The total light

For the light along the major axis decompositions have now been described, which is the most important since the observed spectra are also situated along this major axis. To determine the total light of the bulge and disc, however, one has to know the b/d light ratio for the whole image. It took a small investigation to find a consistent picture for this galaxy.

Near the centre the ellipticity ($a/b = 1/1 - \varepsilon$) indicates a round situation, so at least for $R \lesssim 5''$ the bulge is likely spherical. Inspection of the image in Fig. 1 shows that a hazy component, which may be associated with the bulge, extends to at least half the image of the galaxy and appears to be pretty round. But that is, of course, only limited evidence that the bulge is spherical everywhere. Additional evidence comes from considering the disc.

The velocity field following from the 21 cm emission line gives an inclination of 75° with small error of one to two degrees. The ellipticity a disc with an inclination of 75° would produce is 0.72 for an intrinsic b/a ratio of 0.11 (Guthrie 1992). This differs considerably from the observed ellipticity of 0.60. An explanation for this difference can only be found when NGC 7331 has a bulge which is much rounder than $\varepsilon = 0.60$, producing that observed value in combination with an $\varepsilon = 0.72$ disc. Combination of three pieces of evidence then leads to the conclusion that NGC 7331 has a spherical or nearly spherical bulge and a disc with projected ellipticity of 0.72 as expected for an inclination of 75° . Given the lightprofiles (in the I-band) along the major axis for the three b/d decompositions the total light of bulge and disc can then be calculated and is given in Table 3. Note that to obtain the bulge light the $R^{1/4}$ fit has been integrated till a radius of $150''$; because of this fitting the total light differs slightly for the different decompositions.

5. The model calculations

5.1. Reconstruction of the line profile

The observed spectroscopic data have to be related to the real internal velocity dispersions and stellar rotation of the galaxy. To that aim a 3d model of NGC 7331 will be employed consisting of a disc with a prescribed density distribution and a bulge giving an $R^{1/4}$ law in projection.

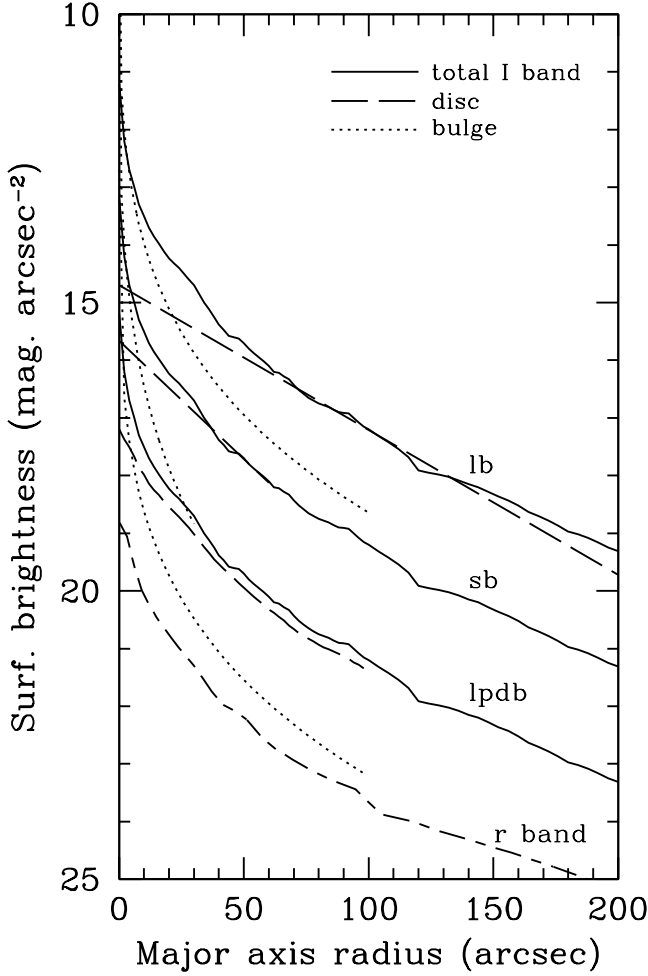


Fig. 7. Elliptically averaged I and r band photometric profiles of NGC 7331. The lower I profile is the actual one, the middle and top I profiles are offset by -2 and -4 mag. and the r -band profile is offset by $+2$ magnitudes. Three bulge/disc decompositions are indicated; lb for a large bulge, sb for a small bulge, and lpdb for a line profile determined bulge situation. In practice the sum of bulge and disc profile is (except for the inner $2''$) indistinguishable from the observed total light profile.

The effect of a dust layer has been neglected, as to the validity of this one is referred to the discussion in Bottema (1989). The observable dispersion generated by the disc is mainly determined by the dispersion in the tangential direction. For the inclination of 75° a small fraction of the perpendicular dispersion enters into the observations and because the disc has a certain thickness, also a fraction of the radial dispersion.

Along the line of sight an integral line profile develops. This process is simulated by numerically integrating the kinematical model of the galaxy. The line profile obtained in that way was then smoothed to the resolution of the restored observations. Next a gaussian and $h3$ parameter

Table 3. Total light of bulge and disc

Bulge type	Disc light ($10^9 L_\odot$)	Bulge light ($10^9 L_\odot$)	b/d ratio
large	10.1	16.2	1.6
small	13.9	9.2	0.7
lpd	12.7	11.4	0.9

were fitted exactly as for the observations. In this way results of the model calculations are precisely comparable to the observational data. Very close to the centre, typically for $R \lesssim 2''$ both, the model calculation and the comparison with observations cannot be done reliably. This is because the integration step was $1''$ the seeing is of the same order and so close to the centre the 3d density distribution of the bulge is not well behaved.

5.2. The disc model

For the disc of NGC 7331 a locally isothermal distribution (Spitzer 1942) with constant thickness has been assumed (van der Kruit & Searle 1982),

$$l_d(R, z) = l_d(R, 0) \operatorname{sech}^2 \left(\frac{z}{z_0} \right), \quad (5)$$

where l_d is the luminosity space density and z_0 indicating the thickness of the disc. In the radial direction the luminosity density was proportional to the surface brightness as given by the dashed lines in Fig. 7, $l_d(R, 0) \propto \mu(R)$. For all cases the value of z_0 has been put at $7''$ which is a compromise between one fifth of the scalelengths (van der Kruit & Searle 1982) of small and large bulge situations. A constant M/L ratio is adopted which gives a vertical velocity dispersion $\langle v_z^2 \rangle^{1/2}$ for the locally isothermal disc of Eq. (5) of

$$\langle v_z^2 \rangle^{1/2} = \sqrt{\pi G z_0 \sigma_0} \sqrt{f(R)} = \langle v_z^2 \rangle_{R=0}^{1/2} \sqrt{f(R)}, \quad (6)$$

with

$$f(R) \equiv \mu(R) / \mu_0. \quad (7)$$

Here σ_0 is the central surface density, $\mu(R)$ the observed (so not corrected to face-on) surface brightness and $\mu_0 = \mu(R=0)$. Note that

$$(M/L)_{\text{disc}} = \sigma_0 / \mu_0^{\text{face-on}}. \quad (8)$$

The velocity dispersion in the radial direction is given by

$$\langle v_R^2 \rangle^{1/2} = \frac{1}{0.6} \langle v_z^2 \rangle^{1/2}, \quad (9)$$

following from observations of old disc stars in the solar neighbourhood, comparison of velocity dispersions of inclined and face-on galaxies (Bottema 1993), and by results

from numerical heating experiments (Villumsen 1985). Finally the velocity dispersion in the tangential direction follows from

$$\frac{\langle v_{\Theta}^2 \rangle^{1/2}}{\langle v_R^2 \rangle^{1/2}} = \sqrt{\frac{B}{B-A}}, \quad (10)$$

where A and B are the Oort constants, which can be derived from the rotation curve. The local velocity distribution is assumed to be gaussian in the three directions.

The input stellar rotation curve (v_*) is given by the testparticle rotation (v_t , see Sect. 3) diminished with the asymmetric drift of the stars (van der Kruit & Freeman 1986; Binney & Tremaine 1987). For a plane parallel disc this drift ($v_t - v_*$) is given by

$$v_t^2 - v_*^2 = \langle v_R^2 \rangle \left[\frac{-R}{\rho} \frac{\partial \rho}{\partial R} - \frac{R}{\langle v_R^2 \rangle} \frac{\partial}{\partial R} \langle v_R^2 \rangle - \left(\frac{A}{A-B} \right) \right], \quad (11)$$

which, using Eq. (6) and (9) is equal to

$$v_t^2 - v_*^2 = \langle v_R^2 \rangle_{R=0} f(R) \left[\frac{-2R}{f(R)} \frac{\partial f(R)}{\partial R} - \left(\frac{A}{A-B} \right) \right]. \quad (12)$$

Usually one can take the rotation of the ionized gas to represent the testparticle rotation. Definitely for $R \lesssim 40''$ this cannot be done for NGC 7331. To resolve this problem an iterative strategy has been followed. As a first guess, from $60''$ inwards a constant rotational velocity of 250 km s^{-1} was assumed. Observable radial velocities and dispersions were calculated for a certain bulge/disc situation and by comparison with the observations the input testparticle rotation together with the other input parameters were adapted to find a satisfactory fit. It proved possible to fix the input rotation quite independently from these other parameters, to end up at a situation where the testparticle rotation increases gently from 255 km s^{-1} at $R = 70''$ to 270 km s^{-1} near the centre. It will be obvious that only such a global trend can be deduced and no details of the rotation curve.

5.3. The bulge model

The three dimensional density distribution of the bulge is given by Eq. (3), and the ratio of bulge to disc density was fixed by comparing the surface brightness calculated from the model distributions with the actual bulge/disc surface brightness along the major axis as given in Fig. 7. For the bulge kinematics a simple model was assumed. The velocity dispersion is isotropic and constant like an isothermal sphere. The bulge is cylindrically rotating with a rotation curve

$$v_{\text{rot}}^b = v_{\text{max}}^b \sqrt{1 - \frac{d_b}{r} \arctan \left(\frac{r}{d_b} \right)}, \quad (13)$$

where the bulge rotational core radius d_b was kept fixed at $1''$. It finally appeared that the maximum bulge rotation v_{max}^b has to be considerably smaller than the disc rotation, but its value is only loosely constrained. Consequently results and conclusions are not sensitive to any reasonable change of this bulge rotational core radius.

6. Fitting the data for the “large” and the “small” bulge

To start this section a short description will be given of the main effects which there are on the observable quantities when changing a certain input parameter of the galaxy model. Near the centre the bulge always dominates the light and hence the bulge dispersion is fixed by the dispersion observed near the centre. In the outer regions the disc dominates the dispersion but the bulge influence is not negligible. Over there the disc generates a high and narrow line profile while the bulge contributes a broad low level component to the profile. Because of the relatively broad (compared to the disc) instrumental profile this underlying bulge component is easily picked up even if the bulge is weak. One may wonder whether the bulge light continues substantially into the disc region and whether it is not cut off at a certain radius. The optical image of this galaxy argues against such a proposition; the bulge remains visible as a faint haze well until radii where the spectroscopy ends. Simulations with a disc only did not produce detectable asymmetric line profiles. Consequently any asymmetry or large $h3$ value must be generated by an unequal bulge and disc distribution and/or kinematics. Increasing the difference between the disc and bulge rotation increases the observable dispersion in the transition region. In the mean time the observable asymmetry then becomes larger.

First the large bulge situation was considered but it appeared impossible to match the observations. Whatever the testparticle rotation of the disc, the bulge rotation in combination with its light distribution dominate the observable rotation, typically for radii $\lesssim 40''$. This results in a rotation much lower than what is observed. The dispersion was always too large between radii of 20 to $80''$ even when the disc dispersion was made very small. In addition, the $h3$ parameter could never be made large enough. To summarize: a large bulge situation is really out of the question.

Next the small bulge was considered. The model parameters were adjusted to obtain the best fit to the observations of which the result is shown in Fig. 8 and 9 for the dispersion and asymmetry respectively. This best fit has a central disc dispersion $\langle v_R^2 \rangle_{R=0}^{1/2}$ of $125 \pm 25 \text{ km s}^{-1}$, a bulge dispersion of $125 \pm 10 \text{ km s}^{-1}$ and bulge rotation of approximately 30 km s^{-1} . For a comparison of model and observed radial velocities and determination of the input testparticle rotation one is referred to the next section and Fig. 14, because results concerning these

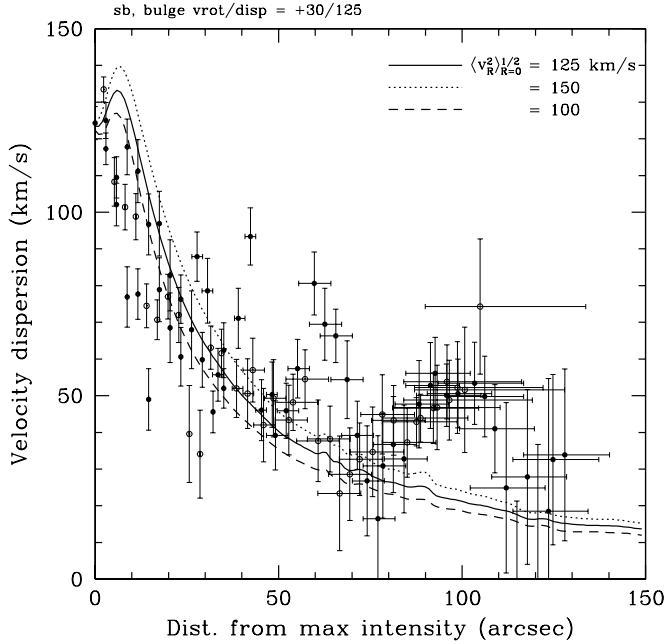


Fig. 8. Comparison of velocity dispersions obtained from a model calculation (the lines) with the observed stellar velocity dispersions. All for a small bulge light decomposition, a bulge rotation and dispersion of 30 and 125 km s^{-1} respectively. A best fit is for a disc central dispersion in the radial direction ($\langle v_R^2 \rangle_{R=0}^{1/2}$) of 125 km s^{-1} . The fit is reasonable but not perfect.

matters are equal for the small and lpd bulge. There appears to be a reasonable resemblance in figures 8 and 9 between the data and the model, but the fits are certainly not perfect. For instance the model dispersion decreases nicely with radius, but too steeply compared to the observations. At the smaller radii, typically for $R \lesssim 30''$ the fitted dispersion is somewhat too large while for radii $\gtrsim 30''$ it is too small. The $h3$ parameter (Fig. 9) also follows the data, but the model values are a factor two smaller than the observations. One can make a larger $h3$ parameter by lowering the bulge rotation to zero or to negative values (= counterrotation). But then also the dispersion values at the transition region between bulge and disc at $R \sim 10''$ increase and that is not consistent with the observations. Already for the present best fit situation for the small bulge the model dispersion is a bit too large at $R \sim 10''$ so that one would prefer a larger bulge rotation, but then the $h3$ parameter gets smaller. Lowering the disc dispersion to decrease the dispersion at the transition region gives too low dispersions at large radii and is not a solution to the problem.

Several combinations of input parameters have been investigated, and the final best fitting result is given in Figures 8 and 9, a result which is not perfect and not satisfactory. The experience obtained when doing these fits for the small bulge situation paved the way towards

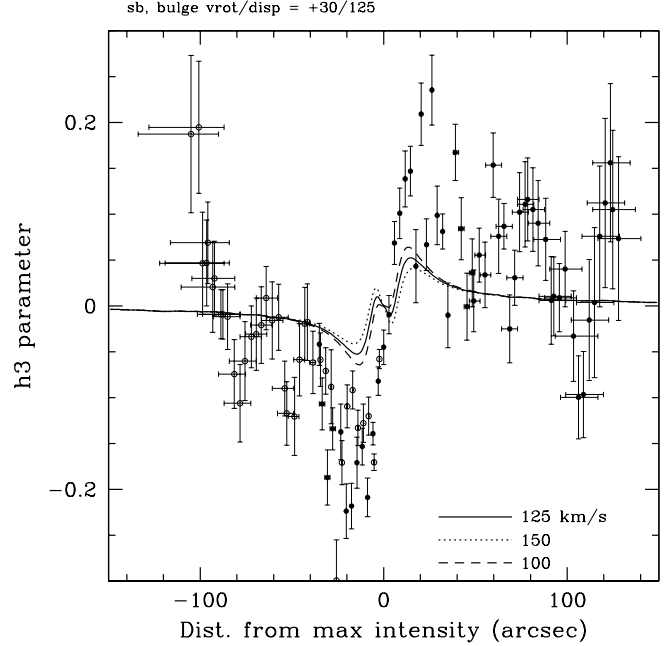


Fig. 9. As Fig. 8, but now for a comparison of model and observed asymmetry parameter. Although the radial functionalities agree, the model asymmetry parameter is too small by a factor of two.

a better solution. It became clear that in order to get a larger $h3$ parameter a comparable bulge and disc intensity is needed over a larger range of radii. The largest asymmetry is there where the intensities are equal and the observations then indicate that this is between radii of 10 to 20''. Considering this, a larger effective radius of the bulge is needed, but the bulge should be less bright than for the large bulge situation. Plotting of the model profiles at diverse radii showed that the individual contributions to this profile of bulge and disc can be distinguished and traced as a function of radius. This knowledge was applied to the observed profiles and it became clear that these too contain information about relative brightness of bulge and disc, leading to the construction of the lpd bulge situation.

7. Fitting the data for a “lpd” bulge

As in the previous section various combinations of input parameters have been investigated. Comparison with the observations gave the best fit which is shown in figures 10 and 11 for the dispersion and asymmetry parameter as a function of radius. The central dispersion in the radial direction ($\langle v_R^2 \rangle_{R=0}^{1/2}$) was determined at $140 \pm 30 \text{ km s}^{-1}$ for a bulge rotation and dispersion of 30 and $125 \pm 10 \text{ km s}^{-1}$. This last value is fixed unambiguously because the bulge dominates the light near the centre. Although a perfect fit could not be achieved for this bulge/disc decomposition, results are better than for the small bulge situation. A larger asymmetry parameter is obtained more in accordance with the observations. In addition the radial

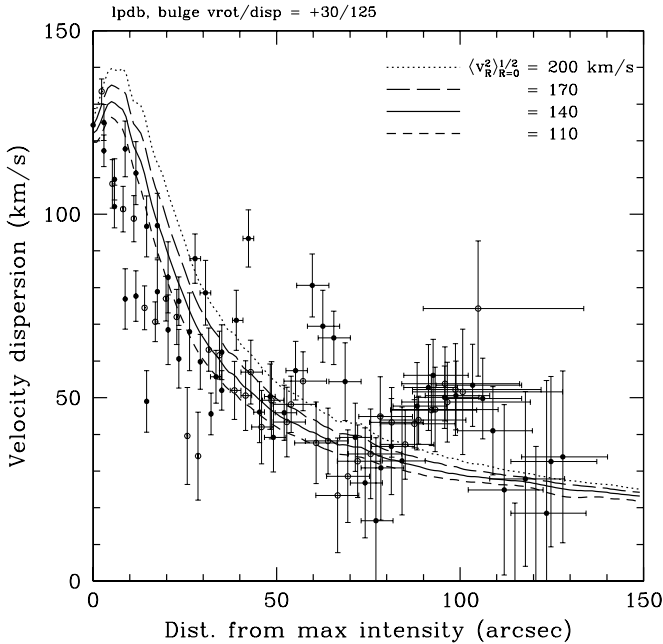


Fig. 10. Comparison of velocity dispersions obtained from a model calculation with the observed velocity dispersions. In this case for an “lpd” bulge/disc light decomposition and a bulge rotation and dispersion of 30 and 125 km s⁻¹ respectively. The best fit for $R > 25''$ is for $\langle v_R^2 \rangle_{R=0}^{1/2} = 140 \pm 30$ km s⁻¹ and shows a better agreement with the data than for the small bulge situation. For $R \lesssim 25''$ a somewhat smaller dispersion is preferred.

behaviour of the dispersion follows the data reasonably well.

The rotation of the bulge is not so well constrained. Effects of a different bulge rotation are shown in figures 12 and 13. Again the same trends as described in the previous section are apparent; a lower bulge rotation gives a larger $h3$ parameter and larger dispersion at radii between 5 to 20'' where bulge and disc are comparable in brightness. For a bulge counterrotating with 20 km s⁻¹ a good fit is found to the asymmetry parameter, but the dispersions around 10'' are considerably larger than what is observed. When the bulge rotates with 80 km s⁻¹, the fit to the dispersions is perfect, but $h3$ values are too small. Therefore a compromise is found for a bulge rotation of $30 \pm \sim 30$ km s⁻¹. In this respect it should be noted that the observed velocity dispersion is more trustworthy than the observed $h3$ parameter, because the latter is more susceptible to small scale irregularities. For instance the small gully on the high and low velocity side of the line profiles (Fig. 4) may have caused the $h3$ values to be determined somewhat too large. The velocity dispersion is always a more global parameter.

Does the fact that the observed $h3$ parameter can only be explained by a bulge counterrotating with 20 km s⁻¹ prove that NGC 7331 indeed has a counterrotating bulge?

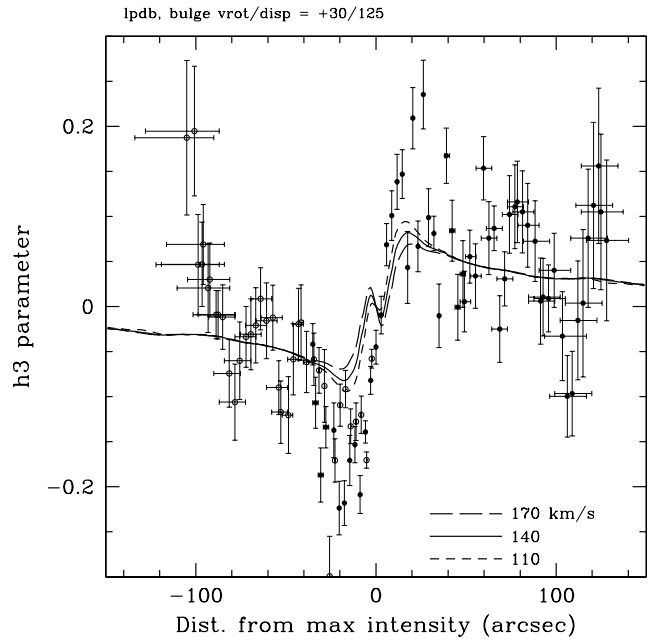


Fig. 11. As Fig. 10, but now for a comparison of model and observed asymmetry parameter. Note that considerably larger $h3$ values can be obtained than for the small bulge model.

If such a situation as explained above and illustrated in Fig. 13 is valid, it is totally different from the counterrotating bulge as proposed by P96. That bulge is cold and counterrotates with ~ 50 km s⁻¹, while the present bulge is hot (disp = 125 km s⁻¹) and counterrotates with only 20 km s⁻¹. Some test line profile calculations have been done for a cold counterrotating bulge. As can be expected in the inner 5'' the calculated dispersion is much lower than observed and between 8'' and 25'' the dispersion is much larger than observed. The $h3$ parameter is irregular as a function of radius and even has the wrong sign at certain positions. Thus a cold counterrotating bulge cannot be made in agreement with the observed kinematics. Instead of a completely counterrotating bulge one might argue for a counterrotating component inside this galaxy. This is not easy to investigate because a spatial distribution for such a component can only be guessed. In any way, such a component would increase the dispersion at the positions where it is situated, which is difficult to reconcile with the observed dispersions. Still, a small counterrotating component inside the bulge or at the bulge/disc transition region cannot completely be excluded. Also judging the fits in Fig. 12 and 13 a slowly counterrotating hot bulge might just be possible.

When the fit to the dispersion in Fig. 10 is considered in detail one can note the following. For $R \gtrsim 25''$ by minimizing the difference between model curves and data there is an excellent fit to the data for $\langle v_R^2 \rangle_{R=0}^{1/2} = 140 \pm 30$ km s⁻¹. However for $R \lesssim 25''$ one would prefer

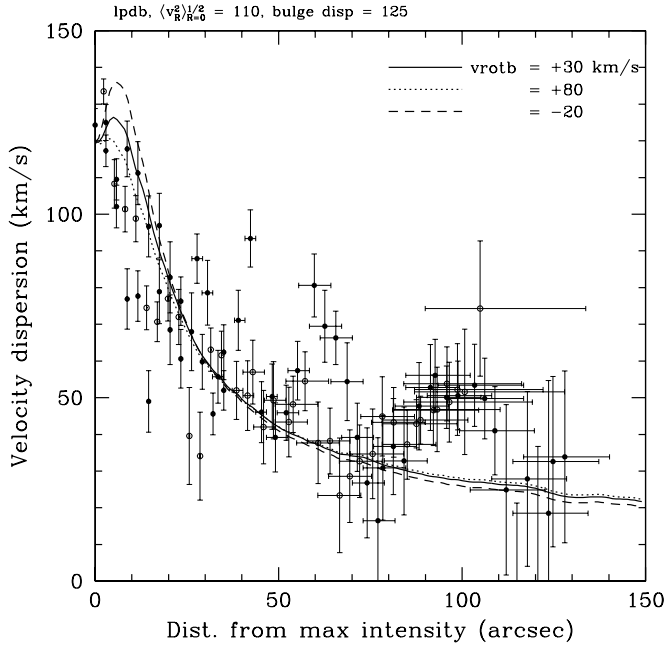


Fig. 12. Illustration of the effects of a different bulge rotation on the observable dispersions. A larger difference between bulge and disc rotation gives a larger dispersion in the bulge/disc transition region.

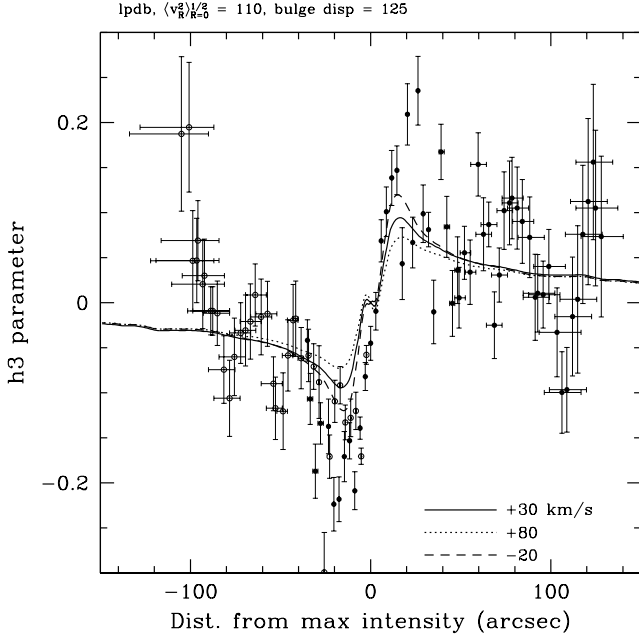


Fig. 13. As Fig. 12, but now for the asymmetry parameter. A larger difference between bulge and disc rotation gives a larger asymmetry of the profile. As a compromise between the fits in figures 12 and 13 a bulge rotation of $+30 \text{ km s}^{-1}$ has been adopted, a value with an appreciable error. Nevertheless, in any case the bulge needs a considerably lower rotation than the disc to explain the observed asymmetric profiles.

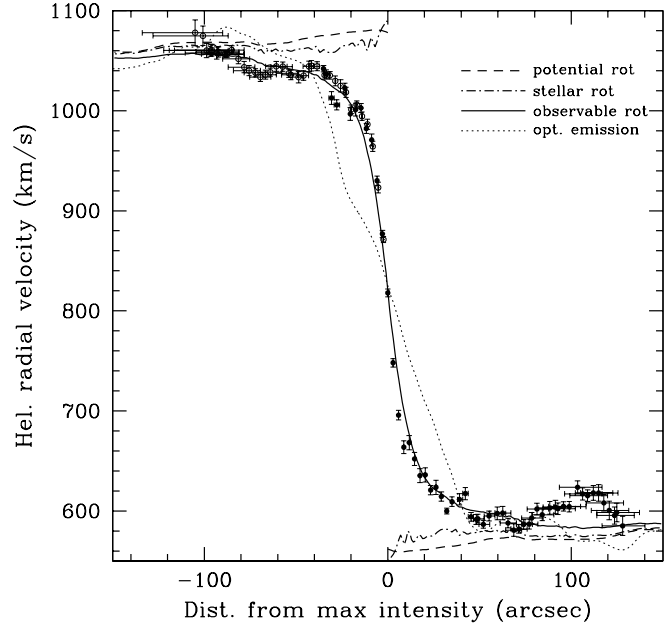


Fig. 14. Comparison of the radial velocities following from the model calculations with the observed stellar radial velocities (for $\langle v_R^2 \rangle_{R=0}^{1/2} = 140 \text{ km s}^{-1}$, bulge rotation and dispersion of $+30$ and 125 km s^{-1} respectively). The input potential rotation was adapted to achieve the best fit.

a smaller disc dispersion: $\langle v_R^2 \rangle_{R=0}^{1/2} = 110 \text{ km s}^{-1}$ or even as low as 80 km s^{-1} . Then, not only the fit to the dispersion is better, but also, as can be seen in Fig. 11, the line profiles are more asymmetric resembling more what is observed. But can this be done, such a smaller dispersion in the inner region? In principle the dispersion over the whole radial extent is fixed by the disc surface brightness through Eqs (6), (9), and (10). But this assumes that the vertical scale parameter (z_0) is the same at all radii. If z_0 can be made smaller for $R \lesssim 25''$ then the dispersion can also be made smaller while remaining consistent with the photometry. This is not even such a bad idea, in fact it is something which might be expected. Inwards of $R = 25''$ one is entering the bulge region where gas is sparse and star formation has nearly ceased. Consequently there will be no spiral arms and no molecular clouds and the disc is prohibited from heating up (Lacey 1991). The disc then remains colder and thinner than at those radii where there is star formation or where star formation has existed longer. Such a lower value of z_0 at or near the bulge would obviously go undetected in observations of edge-on galaxies. Certainly the kinematic data of NGC 7331 can be explained better by a thin and cold disc within the bulge. This fact, however, is not an overwhelming evidence for making thin and cold discs within bulges into a general hypothesis.

In Fig. 14 the radial velocities following from the model calculations are compared with the observed radial veloc-

ities. As described above, there is the freedom to choose the testparticle (potential) input rotation such that the calculated radial velocities match the observations. Thus a comparison of radial velocities cannot give an extra constraint on the velocity dispersion of the disc or on the bulge rotation. What can be concluded from Fig. 14 is that a testparticle rotation curve can be constructed which gives a consistent picture; in this case for $\langle v_R^2 \rangle_{R=0}^{1/2} = 140 \text{ km s}^{-1}$.

The lpd bulge decomposition enables a reasonable reconstruction of the observations. It is likely that an even better fit can be made for slightly different bulge/disc decompositions, for instance for bulges which have brightness laws other than the $R^{1/4}$ employed so far. But the parameter space which then opens up is so vast that a huge amount of time is needed to investigate; while only giving marginal improvements.

Some problems have to be discussed, however. Changing the brightness ratio of model disc and bulge has a considerable effect on the dispersions in the disc dominated region. How well can one then constrain the dispersion of the disc? Fortunately this appears to be a smaller problem than expected. This is because the bulge/disc brightness ratio cannot be changed at will; one has to remain compatible with the observed photometry. In fact, during the construction of the lpd bulge situation an iteration was made to increase the bulge strength with a factor two at the transition radius. Bulge parameters and disc surface brightness then had to be adapted to match the photometry. Surprisingly, the derived disc dispersion turned out to be nearly equal before and after this change. The error generated by the not precisely determined bulge/disc brightness ratio is well comprised within the 30 km s^{-1} error on the value of $\langle v_R^2 \rangle_{R=0}^{1/2}$. Another problem is that the large observed dispersions near $R = 100''$ cannot be explained. Looking at the fit to the data in Fig. 10 this problem looks worse than it is because of the strong oversampling of the data at that radius, caused by the adopted method of averaging along the slit. Taking into account the horizontal error bars which show the amount of oversampling, there are only four independent measurements (two on either side of the galaxy) which have a large dispersion. Still these four measurements cannot be explained by a regular galactic disc situation and consequently the disc is not regular. A hotter disc by a factor of two locally at that radius seems unlikely because then a very local increased heating mechanism must have been present. More likely is a locally irregular stellar velocity field generating broader profiles over the $15''$ spatial resolution at those positions. Evidence supporting this is the discrepant low apparent rotation at $R = 100''$ on the North side only.

8. The amount of mass

8.1. The mass of the disc

The surface density of the disc as a function of radius ($\sigma_d(R)$) is given by

$$\sigma_d(R) = \sigma_0^d f(R) = \frac{(0.6 \langle v_R^2 \rangle_{R=0}^{1/2})^2}{\pi G z_0} \cdot f(R). \quad (14)$$

When substituting $\langle v_R^2 \rangle_{R=0}^{1/2} = 140 \pm 30 \text{ km s}^{-1}$ for the derived disc dispersion and $7'' = 506 \text{ pc}$ for the value of z_0 a central surface density σ_0^d of $1027 \pm 440 M_\odot \text{ pc}^{-2}$ is found. Using Eq. (8) and $\mu_0|_{\text{face-on}} = 18.67 \text{ I-mag. arcsec}^{-2}$ the mass-to-light ratio of the disc is $1.6 \pm 0.7 M_\odot/L_\odot^I$.

Some parameters entering into the calculation of surface density and M/L ratio have not been measured but are inferred from other studies. For example the factor 0.6 which might have a typical error of 0.1; the value of z_0 having some 20% error and there is the uncertainty of the correction to face-on surface brightness which is at present a simple $\cos(\text{inclination})$ factor. Nevertheless, NGC 7331 is a regular galaxy so that one may assume that these parameters have been given the appropriate value. The dominant source of errors is that of the dispersion anyway.

For a number of galactic discs stellar velocity dispersions have now been determined (Bottema 1993). Combining these results leads to a disc M/L ratio of 1.8 ± 0.4 in the B-band (Bottema 1997). The value for NGC 7331 of 1.6 ± 0.7 in the I-band is then consistent with the results for other galaxies under the likely assumption that the B-I colour of the disc of NGC 7331 is comparable to the solar value. This gives confidence that determined and assumed parameters for NGC 7331 are correct.

From the surface density as a function of radius the rotation curve has been calculated (Casertano 1983) which is shown in Fig. 15. The maximum rotation contributed by the disc is 102 km s^{-1} at a radius of 3.8 kpc and the total mass of the stellar disc amounts to $17.8 \cdot 10^9 M_\odot$.

8.2. The rotation curve fit

The rotation curve for NGC 7331 is presented by the dots in Fig. 15, and is given by the HI rotation for $R \gtrsim 70''$ and by the iteration procedure to fit the stellar rotation for $R \lesssim 70''$. The contribution to the total rotation of the disc is fixed by the observed dispersions, and the contribution of the gas is given by the amount of HI and He gas (Begeman et al. 1991). In order to obtain the observed rotation a contribution of the bulge has to be added, and to maintain the flat level at large radii a dark halo has to be invoked. For this dark halo a spherical pseudo isothermal sphere is assumed (Carignan & Freeman 1985) with density law

$$\rho(r) = \rho_0^h \left[1 + \left(\frac{r}{r_{\text{core}}} \right)^2 \right]^{-1}, \quad (15)$$

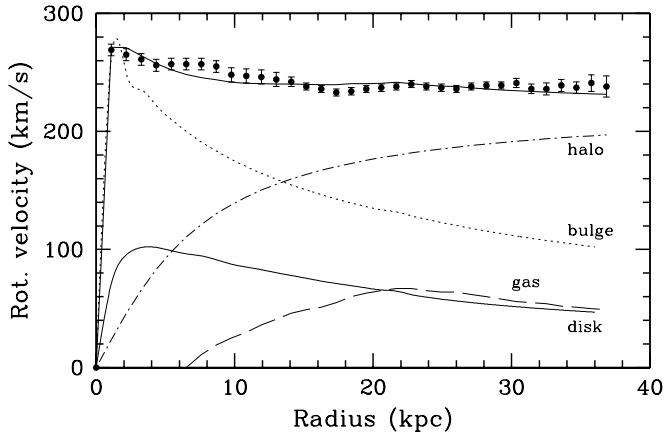


Fig. 15. Fit of the rotation curve of bulge and halo to the observed rotation curve given by the dots. The rotation curve of the disc is fixed by the observed stellar velocity dispersions. Fit parameters are given in Table 4. As can be seen, the bulge and halo dominate the mass distribution at all radii.

and rotation

$$v_h(r) = v_{\max}^h \sqrt{1 - \frac{r_{\text{core}}}{r} \arctan\left(\frac{r}{r_{\text{core}}}\right)}, \quad (16)$$

where the maximum halo rotation v_{\max}^h and the halo core radius r_{core} are two free parameters which can be adjusted to match the observed rotation. A third free parameter is the total mass of the bulge.

The surface brightness of the (lpd) bulge is given by Eq. (2) and parameters of Table 2. This description is all right for $R \geq 2''$ but, because of the steepness of the $R^{1/4}$ law near $R = 0$ care was taken to use the observed surface brightness for $R < 2''$. For an assumed spherical density distribution a rotation curve for the bulge can then be calculated from the surface brightness and M/L ratio using the equation on page 1310 of Kent (1986). If the M/L ratio of the bulge is taken equal to that of the disk (1.6 in I) then the maximum rotation contributed by the bulge is 125 km s^{-1} at $R \approx 1 \text{ kpc}$.

A least squares procedure was used to fit the quadratic sum of the rotation curves of disc, gas, bulge, and dark halo to the observed rotation. The total mass of the bulge became fixed at $87.3 \cdot 10^9 M_{\odot}$ if the bulge would extend until $R = 300''$ and at $77.7 \cdot 10^9 M_{\odot}$ if it extends until $R = 150''$. For the latter, using the total light from Table 3 one finds a M/L ratio of the bulge of $6.8 M_{\odot}/L_{\odot}^I$, being a factor 4.3 larger than the M/L ratio of the disc. The free parameters of the halo became fixed at $r_{\text{core}} = 5.9 \text{ kpc}$ and $v_{\max}^h = 224 \text{ km s}^{-1}$. The fit of the sum of the rotation curves is shown in Fig. 15, together with the contributions of the individual components.

Looking at Fig. 15 it is obvious that bulge and dark halo dominate the potential for the whole galaxy and the

disc only provides a minor contribution. If the M/L ratios of bulge and disc are fixed to be equal then, in addition to providing the rotation at large radii, the halo has to provide most of the rotation at small radii, leading to a very small core radius. Such a scenario is not very realistic. For the free fit of the three parameters, the bulge mass is always determined nearly completely by the innermost rotation points. Changing, for example, the M/L ratio of the disc to 2.5, the maximum allowed by the error on the dispersion, the total bulge mass only decreases from 77.7 to $72.9 \cdot 10^9 M_{\odot}$ but $(M/L)_b/(M/L)_d$ goes down to 2.6 instead of 4.3. A summary of the relevant parameters and fitted values is given in Table 4. There is at least one obvious conclusion following from the rotation curve analysis and that is that a bulge considerably more massive than the disc is needed, having a M/L ratio which is also considerably larger than the disc M/L.

8.3. The mass-to-light ratio of the bulge, a discussion

For the lpd bulge situation a bulge mass-to-light ratio of 6.8 is derived rather independent of the mass of the disc. To obtain a reasonable error on this value, the whole fitting procedure has been repeated for the small bulge situation. This bulge is more compact and hence less mass is needed to bring the rotation to the observed values. In Table 4 the fitted values are presented; the total bulge mass is $40.5 \cdot 10^9 M_{\odot}$ with a M/L ratio of 5.0. A small bulge situation is barely in agreement with the observed dispersions and one may thus consider this M/L ratio of 5.0 as a two sigma deviation from the result for the lpd bulge, leading to $(M/L)_b = 6.8 \pm 1 M_{\odot}/L_{\odot}^I$.

How does this $(M/L)_b$ ratio compare to other M/L ratios? As noted above, it is larger by a factor around four than the disc value of NGC 7331 and the disc value of other galaxies for which stellar velocity dispersions have been measured. But how about (M/L) ratios of bulges of other galaxies? It appears that the literature gives essentially two methods to determine a bulge M/L ratio. At first an application of the Jeans equations to the observed velocity dispersions and morphology. Secondly, when an emission line rotation curve is observed, a fit to that curve can be made by assuming the bulge is the dominant contributor to the rotation in the inner regions.

The first method has been used by Jarvis & Freeman (1985) who used Wilson (1975) two integral distribution function models to fit simultaneously the dispersion, rotation and photometry of three galaxies with large and dominant bulges. This method was also used by Kent (1989) according to the procedure of Simien et al. (1979) which assumes stellar isotropy, to determine the M/L ratio of the bulge of M31. For the second method, the rotation curve fit, one is referred to the papers by Kent (1986, 1987), from which I selected five galaxies with substantial bulges and a well defined bulge/disc decomposition. For the total of nine galactic bulges the M/L ratios are given in Table 5.

Table 4. Rotation curve fit parameters

	lpd bulge (M/L) _d = 1.58	lpd bulge (M/L) _d = 2.5	small bulge (M/L) _d = 1.93 ⁽¹⁾
$M_{\text{disk}} (10^9 M_{\odot})$	17.8	28.1	25.0
$v_{\text{max}}^{\text{disc}} (\text{km s}^{-1})$	102	128	119
$M_{\text{bulge}} (10^9 M_{\odot})^{(2)}$	77.7	72.9	40.5
(M/L) _b	6.8	6.4	5.0
(M/L) _b /(M/L) _d	4.3	2.6	2.6
$r_{\text{core}} (\text{kpc})$	5.9	7.5	3.0
$v_{\text{max}}^{\text{h}} (\text{km s}^{-1})$	224	232	219

(1): All M/L in M_{\odot}/L_{\odot}^I (2): until $R = 150''$ **Table 5.** Bulge M/L ratios

Galaxy	(M/L) _I
NGC 7814	6.1
NGC 4594	4.4
NGC 7123	4.6
M31	3.8
NGC 1353	4.8
NGC 2608	3.5
NGC 2815	7.8
NGC 3200	6.0
UGC 2885	8.2

All listed M/L ratios are converted to the I-band. For the first 3 galaxies an average bulge V-I colour, $\langle V-I \rangle = 1.31$ was assumed according to the colours of a number of dominant bulges in the study of Peletier & Balcells (1997). For the other bulges where a conversion from the r-band to I-band is needed the colour for the M31 bulge was adopted, ($r-I = 1.03$) to be a representative value. In summary, the conversions are $(M/L)_I = 0.58(M/L)_V = 0.42(M/L)_B$ for the first 3 and $(M/L)_I = 0.76(M/L)_r$ for the others. Solar absolute magnitudes are from Worthey (1994) and all mass-to-light ratios are converted to a Hubble constant of $75 \text{ km s}^{-1} \text{ Mpc}^{-1}$. The average $(M/L)_I$ value for the nine bulges in Table 5 is 5.5 ± 0.6 , while the rotation curve fit for NGC 7331 gives $(M/L)_I = 6.8 \pm 1$. Although slightly large, the value of NGC 7331 is in perfect agreement with the M/L's of other bulges.

Now that it has been determined that the mass-to-light ratios of both the bulge and disc are in agreement with M/L ratios of bulges and discs of other galaxies, there is the fact that, in general, M/L's of bulges are larger than those of discs. In numbers one has $(M/L)_{\text{disc}}^I \approx 1.8 \pm 0.4$ and $(M/L)_{\text{bulge}}^I = 5.5 \pm 0.6$, while in the B-band, $(M/L)_{\text{disc}}^B = 1.8 \pm 0.4$ and $(M/L)_{\text{bulge}}^B \approx 13 \pm 1.5$, the difference is even larger. Intuitively one would like to explain the difference by a fading stellar population of the

bulge. That is to say when the bulge is older than the disc its M/L ratio should be larger because the average stellar population is less luminous. For instance Worthey (1994) gives $(M/L)_I$ values for stellar populations. Using solar abundances a population getting older from age = 8 Gyrs to age = 17 Gyrs the $(M/L)_I$ value increases by a factor 1.74. This may not be completely valid for a bulge-disc comparison for various and obvious reasons. Nevertheless this indicative factor 1.74 falls short by nearly a factor of two to explain the observed difference in M/L between bulges and discs. It would be interesting to do a more appropriate population synthesis to see if the observed factor can be explained. If this proves to be impossible, a solution might be to add dark matter, baryonic or non-baryonic, to the bulge. This suggestion has already been put forward to explain the observed large number of lensing events towards the Galactic bulge (Alcock et al. 1997).

9. General discussion and conclusions

In B93, Fig. 1 disc velocity dispersions of 12 galaxies have been plotted versus the absolute luminosity in B of the old disc population. To include NGC 7331 in this sample, first its old disc only absolute magnitude has to be calculated and secondly the radial dispersion at one scalelength. The absolute magnitude for the whole galaxy amounts to -21.73, which is corrected for internal and Galactic extinction and taken from Sandage & Tammann (1981), converted to a distance of 14.9 Mpc. To subtract the light of the bulge the bulge/disc total light ratio of 0.9 in the I-band was converted to a value of 0.56 in the B-band. For this an average bulge B-I colour of 2.3 mag. was assumed, which is the average value of a number of large bulges as observed by Peletier & Balcells (1997), and an average disc B-I colour of 1.8, taken from de Jong & van der Kruit (1994). To get the absolute magnitude of the old disc only, 0.48 mag. was added to the total galaxy value to subtract the bulge light. Then another 0.32 mag. was added to subtract the young disc light (Bottema 1997)

for an estimated B-V disc colour of 0.8. Finally we have $M_{\text{od}}^B = -20.9$ for NGC 7331.

The radial velocity dispersion at any radius is given by $\langle v_R^2 \rangle^{1/2} = \langle v_R^2 \rangle_{R=0}^{1/2} \cdot \sqrt{f(R)}$. To obtain the value at $R = h$, first h was determined as the average of $h = 43''$ (large bulge) and $h = 62''$ (scalelength in outer regions) giving $h = 52'' \pm 10''$. For $\langle v_R^2 \rangle_{R=0}^{1/2} = 140 \pm 30 \text{ km s}^{-1}$ one gets $\langle v_R^2 \rangle_{R=h}^{1/2} = 38 \pm 11 \text{ km s}^{-1}$. If this value is plotted in Fig. 1 of B93 it turns out that the dispersion is low for its brightness; nearly a factor of two lower than the dispersions of other galactic discs. Now the errors are substantial and statistically there is not a disagreement. Still one may wonder about the cause of this low value; several possibilities exist.

Looking at Fig. 10, where the dispersions are given, at $R = h = 52''$ the observed dispersion is $45 \pm 10 \text{ km s}^{-1}$. Assuming the observed dispersion is approximately the tangential dispersion and $\langle v_\Theta^2 \rangle^{1/2} / \langle v_R^2 \rangle^{1/2} = \frac{1}{2}\sqrt{2}$ (for a flat rotation curve), the radial dispersion at $R = h$ should amount to 64 km s^{-1} while in reality the ‘‘input’’ or internal disc value is $38 \pm 11 \text{ km s}^{-1}$. How is that possible? A detailed consideration of the modelling procedure shows that at first some 8 to 10 km s^{-1} can be added to the input value of 38 km s^{-1} caused by integration effects. The remaining 16 to 18 km s^{-1} difference can be accounted for by the bulge. This shows that the bulge still has a considerable effect on the observable dispersion even at one radial scalelength, and that $\langle v_R^2 \rangle_{R=h}^{1/2} = 38 \text{ km s}^{-1}$ is consistent with the observations.

An other reason for the low dispersion might be that the disc of NGC 7331 is not exponential and that instead of $h = 52''$ the scalelength that should have been assumed is smaller, leading to a larger value of $\langle v_R^2 \rangle_{R=h}^{1/2}$. This demonstrates the limitation of the parameterization of the data in Fig. 1 of B93. Therefore presenting an M/L value is better and for NGC 7331 indeed, the derived $(M/L)_I$ of 1.6 is in agreement with values of other galactic discs. On the other hand, it cannot be excluded that a substantial scatter in the $\langle v_R^2 \rangle_{R=h}^{1/2} / \text{abs. mag.}$ relation is intrinsic. This might be caused by a range of edge-on aspect ratios for equal mass discs as a result of different heating rates. That again may be the result of different star formation histories or environment effects. For example the massive bulge of NGC 7331 can have had a profound stabilizing effect on the disc so that less disc heating has appeared.

From the discussion above it is clear that in order to investigate or measure the stellar velocity dispersion of discs it is advisable to observe only galaxies with small bulges. The sample of 12 discs is still small and an extension is needed to make a more accurate determination of the M/L ratio of discs. In addition, or maybe first because it is relatively easy to do, it would be very useful to determine the aspect ratio (or h/z_0) of edge-on galaxies and to find the functionality with disc mass and scatter onto that functionality. That will give insight into the evolu-

tion and star formation history of discs and allow a better interpretation of the disc dispersion/luminosity relation.

Another matter to be discussed is the larger M/L ratio of bulges compared to that of discs. If that is indeed true for most galaxies, there are cosmological consequences. Because bulges are relatively old and have undergone little recent star formation, there must have been a considerable fading over the last 5 Gyrs. That implies that around 5 Gyrs ago, typically at $z \sim 1$ the bulge to disc light ratio must have been larger than presently. Such an effect should be detectable in deep field observations and may compromise galaxy type classification for large look back times.

Finally a compilation of the main conclusions:

1. The determined kinematics of the ionized gas and of the stars is regular and symmetric with respect to the centre of the galaxy.
2. For $R < 40''$ the emission line gas appears to rotate slower than the stars. A likely explanation is an inclined and warped (w.r.t the plane) gas layer in the inner regions.
3. In the bulge dominated region the absorption line profiles are asymmetric; they have a shallow extension towards the systemic velocity.
4. No counterrotating component is observed.
5. Previous claims of a counterrotating component might be based on a wrong interpretation of the data.
6. A galaxy consisting of a bulge and disc with different kinematics is able to explain the asymmetric stellar line profiles.
7. A satisfactory fit to the observed kinematics is found for a rapidly rotating disc with radially decreasing dispersion and a slowly rotating bulge with a constant, 125 km s^{-1} dispersion.
8. An even better fit can be made when the disc is relatively thinner and colder in the bulge region compared to the disc outside the bulge.
9. The bulge influences the observable dispersion to well beyond its light dominated region.
10. The observed disc dispersion gives $(M/L)_{\text{disc}}^I = 1.6 \pm 0.7$, consistent with previous determinations.
11. The bulge mass-to-light ratio is $6.8 \pm 1 M_\odot / L_\odot^I$.
12. The disc contributes only in a minor way to the mass content of NGC 7331.
13. For a sample of discs and bulges one has on average $(M/L)_{\text{bulge}}^I / (M/L)_{\text{disc}}^I = 3.0$ and converted to the B-band $(M/L)_{\text{bulge}}^B / (M/L)_{\text{disc}}^B = 7.2$.

Appendix A: An investigation of UGD and CCC

A.1. A short description of UGD

Suppose the observed absorption line spectrum of a galaxy is given by $G(\lambda)$ and the spectrum of a template star representative of the galaxy’s spectral content is given by $S(\lambda)$.

Then $G(\lambda)$ can be described as a convolution of $S(\lambda)$ with the line of sight velocity distribution, or simply line profile $F(v)$:

$$G(\log \lambda) = \int F(v)S(\log \lambda - v/c)dv, \quad (\text{A.1})$$

where c is the speed of light and conversion to a $\log \lambda$ scale is needed to put the spectrum on a linear velocity scale. To retrieve the line profile $F(v)$ Eq. (A1) has to be inverted. The UGD procedure is one of the methods to accomplish this. It assumes that the line profile can be described by the sum of a collection of equidistant gaussian functions with a fixed dispersion. Then one can solve for the amplitudes of the gaussians that yield a line profile whose convolution with the stellar template S gives the best fit to the observed galaxy spectrum G . This solving is done by a least squares fitting procedure which also gives the errors matching the best fitting line profile. Suppose the dispersion of the gaussians is Δv , then the separation of the gaussians should be not more than $2\Delta v$. Obviously any features on scales less than Δv cannot be retrieved. Here one also has the usual trade-off between resolution and noise; a higher resolution gives a noisier profile and vice versa.

A.2. A short description of CCC

The cross-correlation clean method (CCC) is described in Sect 2.3. In order to invert Eq. (A1) an intermediate step is used by calculating the cross-correlation function (ccf) of the galaxy and template spectrum:

$$ccf = \int G(\log \lambda)S(\log \lambda - \frac{v}{c})d \log \lambda. \quad (\text{A.2})$$

It can be shown (Bottema et al. 1987) that the ccf is equal to the convolution of the line profile and the auto-correlation function of the template spectrum acf_S :

$$ccf = \int F(v)acf_S(\log \lambda - \frac{v}{c})dv. \quad (\text{A.3})$$

This has the advantage that all the absorption lines in the spectrum have been combined in a single peaked ccf; hence the noise is already considerably lower before any fitting or deconvolution procedures are applied. To retrieve the line profile $F(v)$ the ccf is deconvolved using the clean method (Högbom 1974) with the template acf_S as beam (or point spread function). The resolution of the retrieved line profile is uniform and is set explicitly. It can be as high as allowed by the sampling criterion. Again one has the usual trade-off between noise and resolution.

A.3. Testing UGD

When applied to spectra of the inner region of NGC 7331, UGD produces a counterrotating component while CCC

produces only an asymmetric line profile. To investigate this discrepancy both procedures have been tested on a few artificial asymmetric line profiles. This testing scheme is not meant to be an exhaustive investigation, but only to highlight some aspects.

The average template spectrum used for the analysis of the NGC 7331 data (30.2 km s⁻¹ pixel⁻¹, 2040 pixels around 5100 Å) was convolved with an asymmetric line profile. Noise was, or was not, added and the resulting spectrum was considered to be the (test) galaxy spectrum. UGD was then applied using the unconvolved spectrum as template and it was attempted to retrieve the input line profile. The parameters of UGD were equal to those used by P96 and used for the UGD analysis of NGC 7331 described in Sect 3.4; namely a gaussian dispersion of two velocity pixels and a separation of 3 pixels.

For galaxy spectra with no noise added results for three different line profiles are shown in Fig. A1; where the input profile as given by the line is compared with the profile determined by UGD. Formal fitting errors are superposed on the fit, but these are small in this case. In the top panel the input line profile is equal to that generated by the line profile calculation procedure described in Sect. 5, for NGC 7331 with an lpd bulge, $\langle v_R^2 \rangle_{R=0}^{1/2} = 110$ km s⁻¹, $v_{\text{bulge}}^{\text{rot}} = +30$ km s⁻¹, at a distance of 20'' from the nucleus. At that radial distance the observed counterrotating component stands out very clearly. In the middle panel of Fig. A1 a relatively broad profile is shown, while the lower panel depicts the fitting result to a narrow profile with a long one sided extension. As can be seen, UGD gives a good reconstruction of the profiles in the upper and middle panels. The profile in the lower panel, however, is badly reproduced; next to the main profile there have appeared two distinct aliasing features not present in the input profile. But here some care should have been taken that has not been. A part of the input profile is narrower than the UGD resolution and hence UGD can never reproduce the profile. Taking a set of narrower gaussians improves the reconstruction. Unfortunately in practice one has the problem that it is not known in advance how narrow any galactic profile is, consequently making a suitable choice of UGD parameters is not straightforward.

Next noise was added to the artificial galaxy spectra for a S/N level of 20. Results of the UGD reconstruction procedure for the same three input profiles are shown in Fig A2. Now also for the profiles in the top and middle panel the fit starts to deviate from the input; aliasing features are produced on the wing side of the profile. These aliasing features are equal to what may be interpreted as a counterrotating component in a bulge-disc situation. Remember that the top profile is equal to what actually may be expected to occur for NGC 7331 in the ‘‘counterrotating’’ region. Considering the errors, however, these aliasing features are not significant. The correct interpretation of the UGD result should be to disregard these features, but to arrive at this correct interpretation the fit errors have

to be presented. When one has a number of subsequent skewed profiles all having such aliases produced by UGD and no errors are given, a counterrotating component seems to be present, while in reality it is an artifact. This is what may have misled P96 to postulate a counterrotating bulge in NGC 7331.

Lowering the S/N level in general increases the magnitude of the aliases. This can be seen, for example, when comparing the lower panels of figures A1 and A2 where the too narrow profile is presented. A short investigation has been done to see if the UGD fit may be improved when the width and separations of the gaussians are decreased. To that aim Δv was put at $1\frac{1}{2}$ pixel and the separation at 2 pixels and the fitting procedure was rerun for the same profiles and S/N levels. For the no-noise case the reconstruction of the profile in the bottom panel has improved although still some significant aliasing remains. The other two profiles, however, have become somewhat more irregular. When noise is put on for a S/N = 20, in all cases substantial aliasing appears accompanied with a substantial increase of the errors of the fitted profiles. If one had to judge the reconstructed profiles, one would have concluded that the S/N is too low, or a set of wider gaussians is needed.

A.4. The applicability of UGD

Many more tests could have been performed. For instance for different noise levels, for different dispersions and separations of the gaussians, and the effects of template mismatch could have been investigated using an additional different template spectrum. To some this will be interesting but for the present case an adequate explanation of the appearing features has been given.

In fact, the UGD testing as described above is complementary to the test results that KM93 obtained in their original paper describing the method. From that paper it is already clear that problems may arise for skewed profiles. Therefore Kuijken and Merrifield issue two clear warnings when applying UGD:

1. "The errors always have to be superposed on the fit especially for noisy data such that a careful analysis can be made"
2. "The size of the errorbars can be reduced by making the gaussian components broader with a larger separation. However, when the profile is narrower than the gaussians spurious features may be introduced"

In practice the second warning will always cause a problem because one does not know in advance the dispersion of the stellar population or subpopulations investigated. So any small feature generated by UGD needs a further investigation to establish its reality. An additional problem associated with UGD is its hybrid resolution. Features with dispersion less than Δv are unresolved while broader

features are resolved. This may cause problems when interpreting the data.

A.5. Testing CCC

For the same template spectrum and the same three line profiles the CCC method has been investigated. The ccf was calculated between test galaxy and template. This ccf was then cleaned, subtracting components until below the noise level. The line profile was restored by convolving the components with a gaussian having a resolution of $2\frac{1}{2}$ velocity pixels (as for the data analysis of NGC 7331) and by adding the residuals. The errors were determined by measuring the standard deviation in a region on the sides of the profile. That value was assumed to be a representative error for all pixels of the profile. The reconstructed profile should now be equal to the input profile convolved with a gaussian of $2\frac{1}{2}$ pixels. In Fig. A3 this comparison is made for a S/N level of 20. As can be seen, the agreement between input and reconstructed profile is very satisfactory for all three cases. The errors are considerably smaller than those of UGD for the same S/N ratio although a comparison with UGD is not completely fair because UGD tries to reconstruct the profile at full resolution, CCC not. In the middle panel of Fig. A3 one may notice that CCC has the same tendency as UGD to make the profile a bit too narrow in the top. On the other hand, the bottom panel shows that CCC does not give any problems reconstructing extremely narrow and skewed profiles.

Naturally CCC has its disadvantages; the most obvious being that the reconstructed profile is always convolved to a certain (but uniform) resolution. The biggest advantage of the method is that it can be applied without any prior knowledge of the actual galactic line profile. In addition it is straightforward in the sense that no iterative fitting is involved.

Acknowledgements. The observations presented in this paper are obtained with the Isaac Newton Telescope which is operated on the island of La Palma by the Isaac Newton Group in the Spanish Observatorio del Roque de los Muchachos of the Instituto de Astrofísica de Canarias. Many thanks to Jan Lub, who did the actual observations during my unforeseen absence. I also thank Konrad Kuijken for reading the manuscript and I thank him and Joris Gerssen for helpful discussions. The Kapteyn Institute is acknowledged for hospitality and support.

References

- Afanasiev V.L., Sil'chenko O.K., Zasov A.V., 1989, A&A 213, L9
 Alcock C., Allsman R.A., Alves D., et al., 1997, ApJ 479, 119
 Athanassoula E., 1992, MNRAS 259, 345
 Begeman K., 1987, Ph. D. Thesis, University of Groningen
 Begeman K., Broeils A.H., Sanders R.H., 1991, MNRAS 249, 523
 Bender R., 1990, A&A 229, 441

- Binney J., Merrifield M., 1998, *Galactic Astronomy*, Princeton Univ. Press, Princeton, NJ
- Binney J., Tremaine S., 1987, *Galactic Dynamics*, Princeton Univ. Press, Princeton, NJ
- Bosma A., 1978, Ph. D. Thesis, University of Groningen
- Bottema R., 1988, *A&A* 197, 105
- Bottema R., 1989, *A&A* 225, 358
- Bottema R., 1993, *A&A* 175, 16 (B93)
- Bottema R., 1997, *A&A* 328, 517
- Bottema R., Gerritsen J.P.E., 1997, *MNRAS* 290, 585
- Bottema R., van der Kruit P.C., Freeman K.C., 1987, *A&A* 178, 77
- Braun R., Walterbos R.A.M., Kennicutt R.C., 1992, *Nat.* 360, 442
- Boulesteix J., Georgelin Y.P., Lecoarer E., et al., 1987, *A&A* 178, 91
- Carignan C., Freeman K.C., 1985, *ApJ* 294, 494
- Casertano S., 1983, *MNRAS* 203, 735
- de Jong R.S., van der Kruit P.C., 1994, *A&AS* 106, 451
- Dalcanton J.J., Spergel D.N., Summers F.J., 1997, *ApJ* 482, 659
- Efstathiou G., Lake G., Negroponte J., 1982, *MNRAS* 199, 1069
- Franx M., Illingworth G.D., 1988, *ApJ* 327, L55
- Guthrie B.N.G., 1992, *A&AS* 93, 255
- Högbom J.A., 1974, *A&AS* 15, 417
- Hohl F., Zang T.A., 1979, *AJ* 84, 585
- Hughes S.M.G., Han M., Hoessel J. et al., 1998, *ApJ* 501, 32
- Illingworth G.D., Freeman K.C., 1974, *ApJ* 188, L83
- Jarvis B.J., Freeman K.C., 1985, *ApJ* 295, 324
- Jore K.P., Broeils A.H., Haynes M.P., 1996, *AJ* 112, 438
- Katz N., Gunn J.E., 1991, *ApJ* 377, 365
- Kent S.M., 1986, *AJ* 91, 1301
- Kent S.M., 1987, *AJ* 93, 816
- Kent S.M., 1989, *AJ* 97, 1614
- Kormendy J., Illingworth G., 1982, *ApJ* 256, 460
- Kuijken K., 1993, *PASP* 105, 1016
- Kuijken K., Merrifield M.R., 1993, *MNRAS* 264, 712 (KM93)
- Lacey C., 1991, in: Sundelius B. (ed), "Dynamics of Disc Galaxies", Dep. of Astronomy/Astrophysics, Göteborgs Univ. and Chalmers Univ. of Technology, Göteborg, p. 257
- Merrifield M.R., Kuijken K., 1994, *ApJ* 432, 478
- Miller R.H., Smith B.F., 1979, *ApJ* 227, 785
- Mo H.J., Mao S., White S.D.M., 1997, *MNRAS* in press
- Ostriker J.P., Peebles P.J.E., 1973, *ApJ* 186, 467
- Peletier R.F., Balcells M., 1997, *NewA* 1, 349
- Prada F., Gutierrez C.M., Peletier R.F., McKeith C.D., 1996, *ApJ* 463, L9 (P96)
- Rhee M.-H., 1996a, Ph. D. Thesis, University of Groningen
- Rhee M.-H., 1996b, *A&AS* 115, 407
- Rix H.-W., White S.D.M., 1992, *MNRAS* 254, 389
- Rix H.-W., Franx M., Fisher D., Illingworth G.D., 1992, *ApJ* 400, L5
- Rix H.-W., Kennicutt R.C. Braun R., Walterbos R.A.M., 1995, *ApJ* 438, 155
- Rubin V.C., Burbidge E.M., Burbidge G.R., Crampin D.J., 1965, *ApJ* 141, 759
- Sandage A., Tammann G.A., 1981, *A Revised Shapley-Ames Catalog of Bright Galaxies*, Carnegie Institute of Washington
- Sargent W.L.W., Schechter P.L., Boksenberg A., Shortridge K., 1977, *ApJ* 212, 326
- Simien F., Pellet A., Monnet G., 1979, *A&A* 72, 12
- Spitzer L., 1942, *ApJ* 95, 239
- Statler T.S., 1995, *AJ* 109, 1371
- Syer D., Mao S., Mo H.J., 1997, *astro/ph9711160*
- Thuan T.X., Gunn J.E., 1976, *PASP* 88, 543
- Tonry J., Davis M., 1979, *AJ* 84, 1511
- Tully R.B., Fisher J.R., 1977, *A&A* 54, 661
- van Albada T.S., Bahcall J.N., Begeman K., Sancisi R., 1985, *ApJ* 295, 305
- van Albada T.S., Sancisi R., 1986, *Philos. Trans. R. Soc. London, Ser. A* 320, 447
- van der Kruit P.C., Freeman K.C., 1986, *ApJ* 303, 556
- van der Kruit P.C., Searle L., 1982, *A&A* 110, 61
- van der Marel R.P., Franx M., 1993, *ApJ* 407, 525
- Villumsen L.V., 1985, *ApJ* 290, 75
- Wilson C.P., 1975, *AJ* 80, 175
- Worthey G., 1994, *ApJS* 95, 107
- Wynne C.G., 1977, *MNRAS* 180, 485
- Young P.J., 1976, *AJ* 81, 807

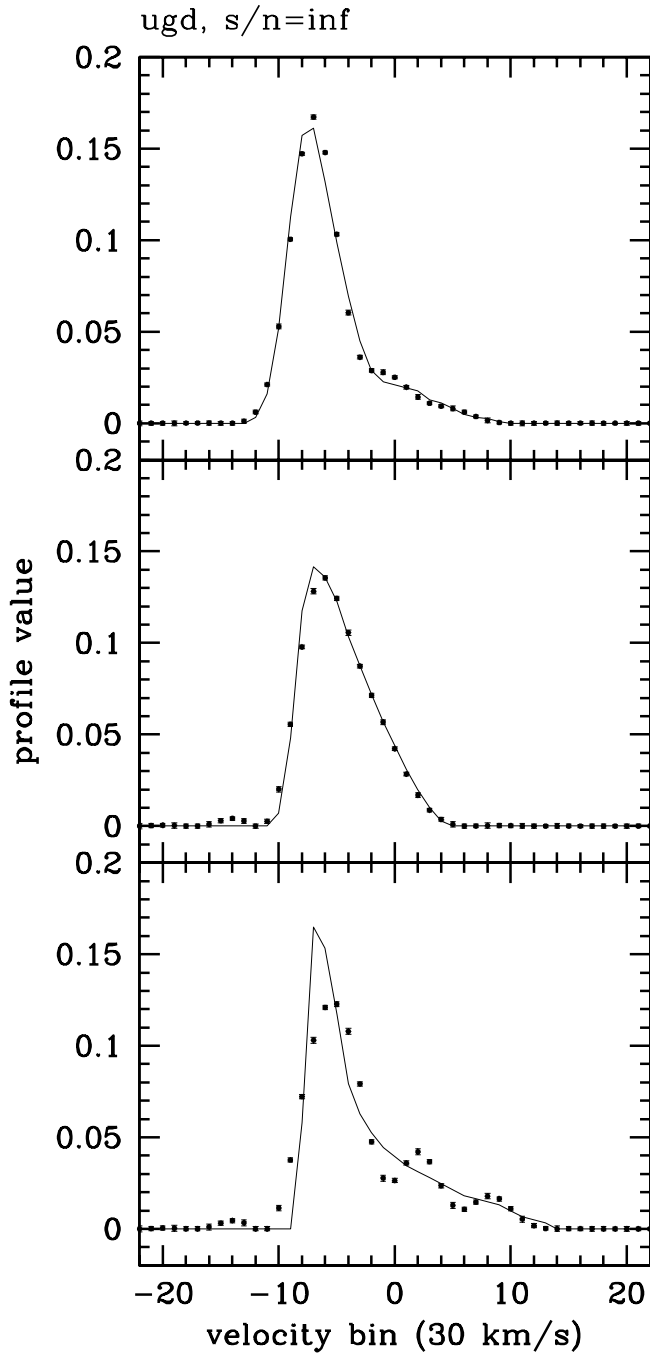


Fig. A.1. Results of the line profile reconstruction using UGD for three different asymmetric input profiles given by the lines. The UGD result is given by the dots. In this case no noise was added to the galaxy spectrum. When the profile is broader than the preset resolution of the method a good reconstruction is obtained. Otherwise (bottom panel) aliases appear.

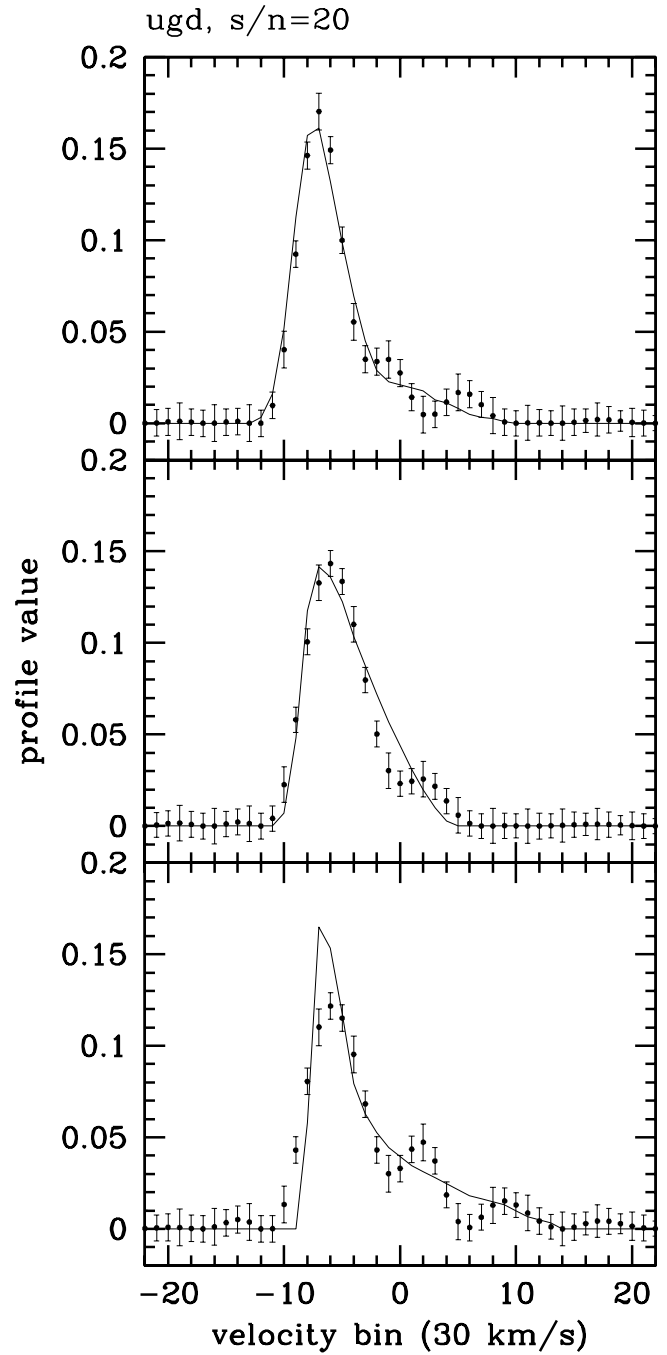


Fig. A.2. As Fig. A1, but now for noise added to the galaxy spectrum for a S/N level of 20. In all cases aliasing is present, though considering the errors, not at a significant level. However, when the errors are omitted one can be made to believe that additional (counterrotating) line profile components are present.

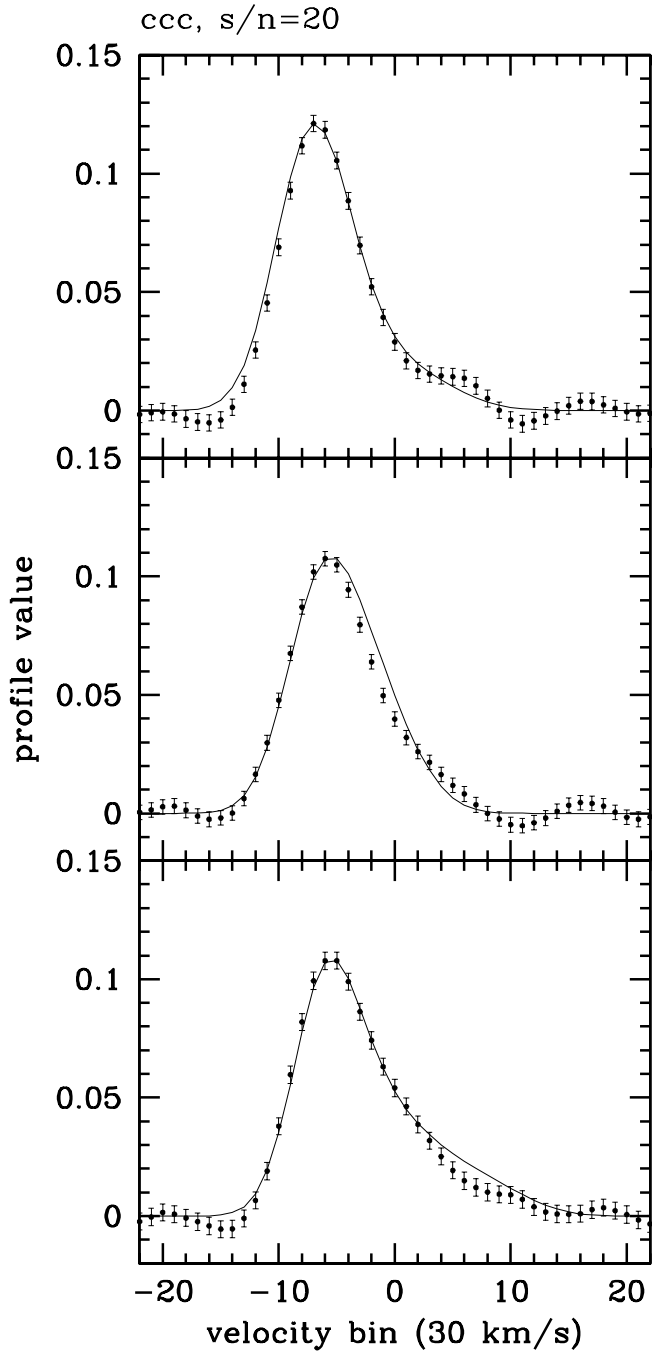


Fig. A.3. Results of the line profile reconstruction using CCC for the same three input profiles as in figures A1 and A2. CCC can only retrieve the profiles convolved with a certain preset resolution. The output profile is thus compared with the input profile convolved to that resolution. In all cases a good reconstruction is achieved.